Electrohydrodynamic (EHD) printing for Advanced Micro/Nano Manufacturing: Current Progresses, Opportunities, and Challenges

Yiwei Han, Jingyan Dong*
Department of Industrial Engineering and Systems Engineering
North Carolina State University
Raleigh, NC, 27695, USA

*: To whom all the correspondence should be addressed, Email: jdong@ncsu.edu

Abstract:

The paper provides an overview of high-resolution electrohydrodynamic (EHD) printing processes for general applications in high-precision micro and nano-scale fabrication and manufacturing. Compared with other printing approaches, EHD printing offers many unique advantages and opportunities in the printing resolution, tunable printing modes, and wide material applicability, which has been successfully applied in numerous applications that include additive manufacturing, printed electronics, biomedical sensors and devices, and optical and photonic devices. In this review, the electrohydrodynamics based printing mechanism and the resulting printing modes are described, from which various EHD printing processes were developed. The material applicability and ink printability are discussed to establish the critical factors of the printable inks in EHD printing. A number of EHD printing processes and printing systems that are suitable for micro/nano manufacturing applications are described in this paper. The recent progresses, opportunities, and challenges of EHD printing are reviewed for a range of potential application areas.

1. Introduction

Fabrication processes that can reliably produce features and structures with micro/nano scale resolution are critically important for micro and nano-scale manufacturing and many other emerging applications. Optical lithography-based micro/nanofabrication processes [1, 2] are widely used in semiconductor industry and researches in micro/nanotechnology. Using a photomask to expose a thin layer of photoresist on the surface of the substrate, state of art lithographic approaches can fabricate features with critical dimension well below 50 nm. Despite

the great resolution capability and high manufacturing throughput, the optical lithographic processes rely on tools with high capital costs, and generally can only produce 2D features from a photomask on a flat substrate using a limited collection of functional materials. Many micro/nano scale material removal processes, such as micro/nano machining and laser micromachining [3-5], also attracted lots of attention due to their great potential in micro/nano manufacturing. These material removal processes utilize various mechanisms and tools, such miniaturized cutting bits (e.g. diamond cutting tools, AFM tips) and lasers, to gradually remove material from the work piece and produce complex 2D and 3D meso/micro/nano structures, which were successfully applied to the medical, aerospace, automotive, consumer electronics and semiconductor industries. However, as subtractive processes, these micromanufacturing approaches still lacks capabilities of multi-material integration, and can only be applied to materials that are machinable.

Printing technologies [6, 7] as additive fabrication approaches, directly deliver functional materials onto the substrate to create 2D patterns and 3D structures, which offer many advantages over other fabrication approaches. With the printing approach, materials of interest can be easily printed into the pre-designed patterns without using a mask, which offers a convenient way for rapid product-development and the manufacturing of complex products with multiple materials. Moreover, printing process can be easily expanded to many unconventional substrates, such as flexible, stretchable, and/or uneven curved substrates. Among many of the developed printing technologies, inkjet printing is a most widely used technology that has been applied to many areas, for example, office, printed electronics, optical devices, and biomedical devices [6-10]. In inkjet printing, the droplets are ejected from the nozzle by the pressure pulses generated from piezoelectric or thermal or pneumatic actuation. The droplets are deposited on a substrate with high spatial control to form the patterns designed by the user. A wide range of ink materials that span from metallic inks, polymers to bio-materials were studied for inkjet printing with demonstrated promising results for different applications. Despite the wide existing applications of inkjet printing, one critical challenge of inkjet printing is its limited printing resolution. The printing resolution in ink-jet printing is mostly determined by the dimension of the printing nozzle, and is typically limited to about 20 μm. Efforts were spent on reducing the nozzle size to obtain smaller droplets. However, the fabrication of the nozzle with micron-scale orifice is challenging and costly [11]. Moreover, reducing the nozzle size for better resolution will require a high actuation effort that is unpractical for many viscous inks, since the printing pressure to form

droplets scales up much faster when the nozzle diameter is decreased according to Hagen-Poiseuille equation. Sub-10μm droplets were seldom reported by inkjet printing [12], in which a highly customize nozzle and ink materials had to be used. Screen printing [13-16], as another commonly used method for pattern transfer, was also demonstrated in high-resolution printing, but special requirements on the inks are needed to achieve the high-resolution capability. Moreover, for the screen printing process, a mask (i.e. stencil) is needed to fabricate the features for each new device design, which make the overall fabrication process time-consuming and not cost-effective.

Electrohydrodynamic (EHD) printing [17, 18], is a high-resolution printing method, which effectively overcomes the limitation in resolution from the nozzle size in inkjet printing. In the EHD printing, the ink material is driven by an electric field, which causes mobile ions in a polarizable liquid to gather at the surface. The Columbic force causes the meniscus at the nozzle end to deform into a conical shape (i.e., Taylor cone). With a large enough electric field, the surface charge repulsion at the cone apex exceeds the surface tension, and a droplet or a jet of fluid is printed onto the substrate (Figure 1). In EHD printing, the droplet/jet is formed by the electric field at the cone tip, and is significantly smaller than the nozzle size, which can overcome the limitation from the nozzle size to achieve better resolution for the production of micro and nano-scale features. Electrohydrodynamic phenomenon was studied long time ago by Zeleny back to 1917 [19], and was then investigated both theoretically and experimentally by numerous researchers, which provided insightful understanding of the phenomenon along with many important applications. Depending on different process configurations, there are different EHD printing modes [20], including widely cited electrospray [21, 22] and electro-spinning [23-26], both of which utilize the unstable electrohydrodynamic behaviors. The regimes of electrospinning and electrospray are affected by different ink properties, such as surface tension and viscosity, and process conditions. In general, from Rayleigh instability, larger surface tension tends to convert the liquid jet into spherical droplets to achieve electrospray. On the other hand, viscoelastic force from the ink viscosity favors the formation of a thin jet to achieve electrospinning. In electrospray, axis-symmetric instability breaks up the jet into numerous tiny droplets, while in electrospinning, non-axis-symmetric instability (i.e. whipping) is experienced by the jet to evaporate the solvent to form solid fibers. These instabilities are necessary for electrospray and electrospinning-based applications but devastating for micro/nano manufacturing of high precision features and structures. Thus, these two processes, electrospray and electrospinning, will not be discussed in

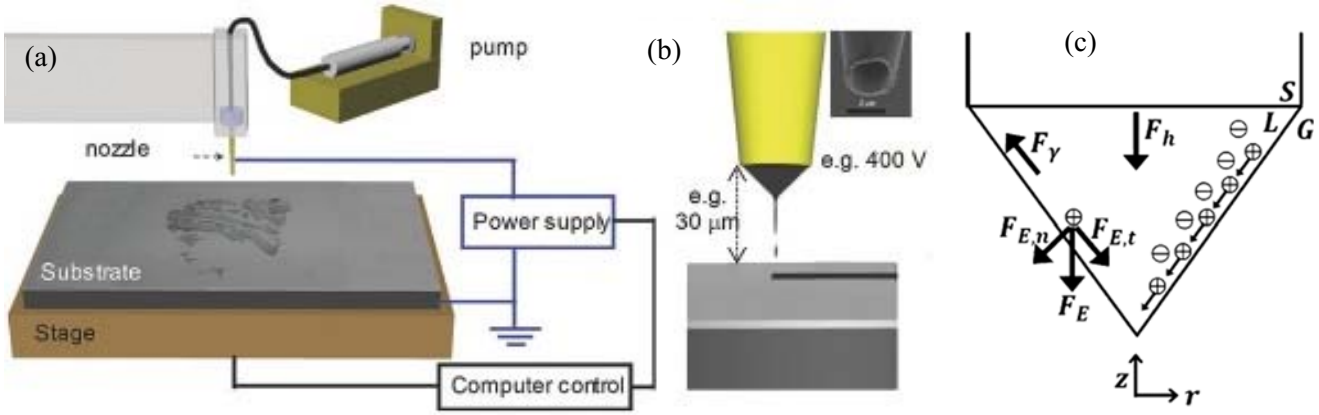

Figure 1: High-resolution electrohydrodynamic (EHD) printing. (a) Schematic illustration of an EHD printing system. A voltage is connected to the nozzle and the electrode under the substrate to eject the ink with electrostatic force. (b) A typical nozzle and substrate configuration for EHD printing. Ink ejects from the apex of the conical meniscus that forms at the tip of the nozzle owing to the action of a voltage applied between the tip and ink, and the underlying substrate. These droplets eject onto a moving substrate to produce designed patterns. Reproduced with permission [17]. Copyright 2007, Nature Publishing Group. (c) Mechanism of EHD printing with typical forces acting on the fluid surface. Hydrodynamic force (F_h), which supplies fluid to the meniscus; the surface tension force (F_γ), which hangs the droplets on the capillary tip; and the electrostatic force (F_E), which deforms the meniscus into the cone shape and eject droplets or jet from the cone tip. S, L, G indicate the solid phase, liquid phase, and the gas phase, respectively. Reproduced with permission [31]. Copyright 2013, American Chemical Society.

this paper. Working in a stable printing region with precisely controlled ink delivery is critical for the precision fabrication using EHD printing. A stable jet mode or pulsating printing mode (i.e. micro-dripping mode, single droplet printed onto the substrate) provide promising potential for the high precision fabrication of micro/nano scale features by printing continuous filaments and/or separated droplets, given that the filament and droplet formation and placement can be precisely controlled. Currently, a variety of materials, such as metallic materials, polymers, biomedical materials, and etc., were successfully applied to EHD printing for many different applications, and the patterning resolution ranging from micron scale to sub-micron scale was successfully demonstrated. With customized nozzles and inks, EHD printing can offer an even higher printing resolution, as high as at the scale of tens of nanometers for bioengineering or electronic applications.

This review covers recent development on EHD printing technology from a manufacturing perspective. In the section 2, the mechanism of the EHD behavior and different EHD jetting modes are discussed to provide insights for process development. Section 3 reviews the required material printability for EHD printing and summarizes the typical functional materials that have already

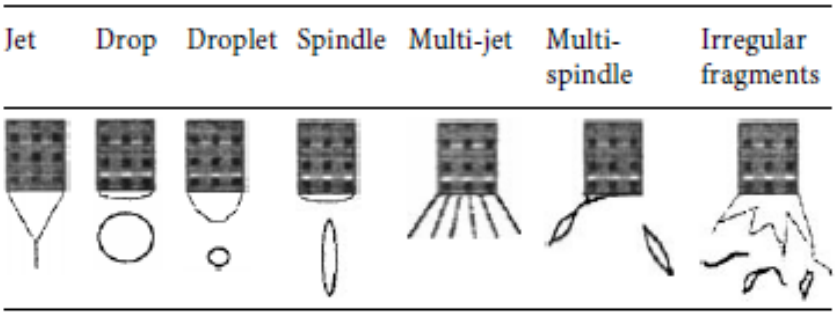

Figure 2: Typical jetting modes of EHD printing. Reproduced with permission [22]. Copyright 1999, Springer Publishing.

been demonstrated for EHD printing. Section 4 discusses the representative EHD printing processes and printing systems, and their capabilities and limitations. In section 5, the theoretical analysis that includes scaling law, numerical and theoretical modeling of EHD printing process is discussed. Section 6 summarizes a few state-of-art applications of EHD printing technology, and then an overview of the EHD printing technology is presented in the final section.

2. EHD Printing Mechanism and Printing Modes

In the typical EHD printing setup, a high voltage is applied between a nozzle (and the ink in the nozzle) and a grounded substrate (Figure 1). The electrostatic force deforms the ink meniscus to form a Taylor-cone. When the electrostatic force exceeds the surface tension and the viscous force of the ink, the droplets or the jet are generated from the apex of the cone [17] The electrohydrodynamic behavior and mechanism of the jet formation have complex and coupled physics, and are affected by ink properties, such as viscosity, surface tension, electrical conductivity or dipole moment, and many process related factors including applied voltage, pressure, and flow rate. Understanding the jet formation and jetting modes can provide practical guidelines for designing the stable high-resolution printing process and selecting the proper printing parameters. Lots of efforts were conducted on both experimental and theoretical aspects to study the EHD jet formation and jetting modes based on the printing parameters and ink properties.

In the EHD printing, along with different printing conditions and material properties of the ink, a number of jetting modes can be observed at the apex of the Taylor-cone [27-30], as shown in Figure 2. Among these modes, dripping mode, microdripping mode, cone-jet mode, and multi-

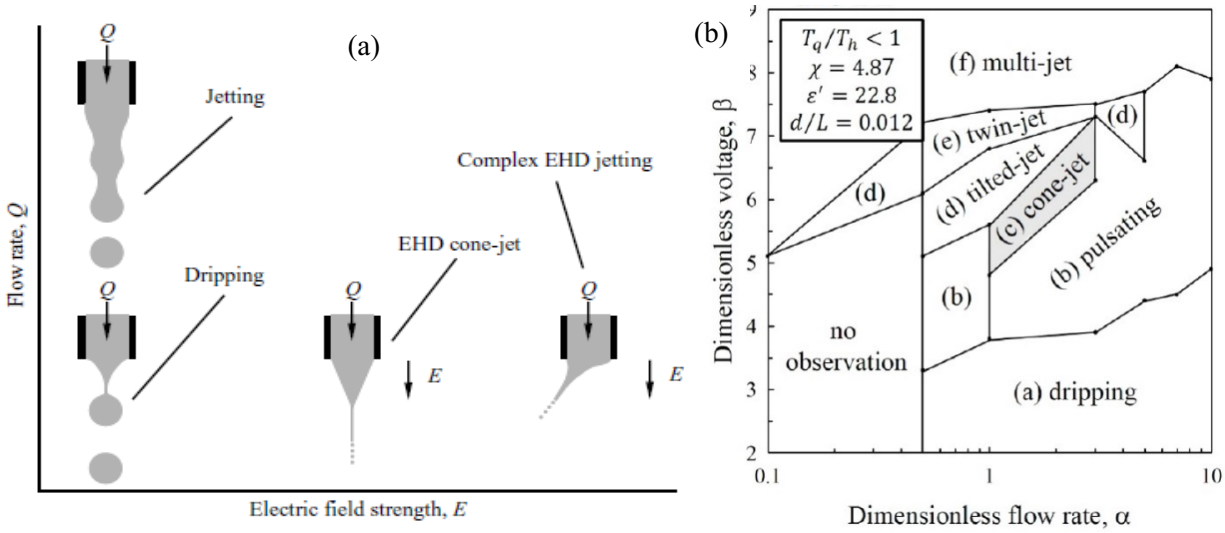

Figure 3: (a) Phase diagram depicting flow transitions that occur as flow rate and/or electric field strength are varied. (b) Jetting maps showing the dependence of jetting modes on dimensionless parameters. Reproduced with permission [31]. Copyright 2013, American Chemical Society.

jet mode are widely observed in the experiments. These modes are generally controlled by the applied voltage and the flow rate of the ink. The dripping mode is usually observed when the applied voltage is relatively low and the printing liquid has a low viscosity, which is very similar to the dripping from a nozzle without any voltage. When the applied voltage is increased, a microdripping mode can be observed. In the microdripping mode, the size of the produced droplet is much smaller than the size of the nozzle. Generally, the microdripping mode occurs only when the ink flow rate and ink viscosity are low. If the flow rate is relatively high, spindle mode can be generated, in which a column of ink is ejected to maintain the flow balance. When the voltage is further increased, and the ink has a relatively high viscosity, the cone-jet mode is formed. In the cone-jet mode, a thin liquid jet is formed at and ejected from the apex of the cone. Increasing the voltage and ink flow rate to a very high value, multiple jets are ejected from the meniscus, which leads to the multijet mode. In the multijet mode, the cone is shrinking and becomes flat, and the printing process is obviously unstable and uncontrollable [20]. When further increase the voltage, satellite droplets or atomization/spraying can be produced. The phase diagram in Figure 3(a) qualitatively shows the relationship between the printing modes and two critical process parameters (i.e. voltage or electric field strength, and flow rate) [31]. Clearly, for precision manufacturing, the micro-dripping mode (i.e. pulsating) and the stable cone-jet mode provide the

required controllability of the printing process, which are used as drop-on-demand printing and direct writing respectively.

The effect of the process parameters that included ink properties, printing and environmental conditions, and nozzle geometry on the jetting behavior [31-33] were systematically studied by a few groups. A dimensionless analysis was performed by Ahn's group [31] to figure out a map of the jetting modes with respect to the ink properties and printing conditions. With the Buckingham π theorem, ten key variables associated with the ink properties and the printing parameters were identified and six dimensionless number (D_1 to D_6) governing the EHD printing system were systemized. The six dimensionless number were derived as D_1 to D_6 = $\left\{ \frac{\varepsilon_0 \varepsilon' Q_s}{d^2 L K}, \frac{(\gamma^2 \rho \frac{\varepsilon_0 \varepsilon'}{K})^{1/3}}{\eta}, \varepsilon', \frac{d}{L}, \frac{\rho K Q_s}{\gamma \varepsilon_0 \varepsilon'}, \frac{\varepsilon_0^{0.5} V_a}{(\gamma d)^{0.5}} \right\}$, where ρ is the density of the ink, ε_0 is the permittivity of free space, ε' is the permittivity of the fluid, K is the conductivity, η is the viscosity, d is the nozzle diameter, L is the distance between nozzle and counter electrode, Q_s is the supplied flow rate, and V_a is the applied voltage. These dimensionless numbers include dimensionless time (D_1), dimensionless material properties (D_2 and D_3), dimensionless geometry (D_4) , dimensionless flowrate (D_5), and dimensionless voltage (D_6), which are variables related to properties of the ink, geometry of the printing system, and processing conditions. Printing behaviors affected by different dimensionless numbers were characterized for a set of inks with various material properties. These inks were obtained by mixing two organic solvents, ethanol and terpineol, with different ratios. A constant DC voltage was applied for the printing process, and a high-speed camera was used to observe the printing process and the resulting jetting modes. Based on the experimental observation, the jetting map for each ink was developed as a function of the dimensionless voltage and dimensionless flow rate, as shown in the Figure 3(b). This approach provides a systematic way to find the processing windows of the EHD printing. The control of the ink properties with the optimized process parameters will help to guide the process design for improved jetting performance. Besides the ink properties and printing parameters, it was found that environmental conditions could also affect the printing behavior and the jetting mode [32, 33]. For a surrounding gas with lower breakdown potential than that of the printing materials, such as He or Ne, electrohydrodynamic spraying cannot be triggered. The importance of the ink

conductivity was studied by [32, 33], and it was discovered that insulating liquids such as paraffinic oils cannot have a stable jetting, and the stable jetting was only formed for liquids with leaky dielectrics at a sufficient voltage level. Other research on the jet formation or the jetting modes included studying on the jetting formation with dielectric liquids, determining the flow rate for EHD cone-jet printing, and the amount of charges on the Taylor cone [34-36]. Scaling laws for the minimum flow rate (Q_m) of the stable cone-jet mode were studied. It was found that the well-known scaling law $Q_m \sim \frac{\varepsilon\gamma}{\sigma\rho}$ (ε, γ, σ, ρ are permittivity, surface tension, electrical conductivity, and density of the working fluid respectively) that is proportional to the charge relaxation time and independent of the nozzle diameter is only applicable to lowly viscous systems. For high viscosity liquids, it was discovered that the minimum flow rate appears to scale as $Q_m \sim \frac{\gamma D^2}{\mu}$ that is proportional to the capillary-viscous velocity (γ/μ with μ as ink viscosity) and the cross-sectional area of the nozzle (D), but independent of the liquid conductivity [34], which gave a guideline on selecting the process conditions for high viscosity inks.

Among all these jetting modes, the micro-dripping mode (i.e. pulsating mode) received significant attention from researchers, as it provides well-controlled drop-on-demand printing capabilities. Many researches were conducted to understand the jet behavior and droplet formation by studying the pinch-off or the break-up behavior of the pulsating EHD printing [37-41]. Zhang's group studied the pinch-off behavior at the dripping mode using a viscous ink and a highly conducting ink [37]. It was found that with increased electric field strength, the volume of the droplet decreased but the thread length (length of the thin liquid filament that connects the meniscus at the nozzle tip and the ejected droplet) increased. The threads always ruptured at the upstream end of the jet when the liquid was subjected in high electric field strength. The satellites were formed directly from the thread, which represented an unstable printing behavior. The ink properties have a significant impact on the pinch-off behavior, as studied by [38]. In this study, the effects of electrical conductivity, charge level, and surface tension of a few inks on the pinch off behavior of the EHD printing were investigated. The range of the dimensionless charging level was obtained for achieving a stable printing condition. The same jetting behavior was observed

for a variety of inks, when the dimensionless charging level and electrical conductivity were the same.

In traditional EHD printing, a constant voltage is applied between the nozzle and the ground electrode, in which, the pulsating frequency and the droplet size are both related to the applied voltage. To improve the controllability of the printing process, pulsed voltage was utilized to drive the printing process, which makes the droplet generation and ejection quite different from the EHD printing using the constant DC voltage. The EHD jetting mode using a pulsed-DC voltage was studied by [42], in which the jetting behavior under different pulse duration were captured with a high-speed camera. The results indicated that the jetting modes were affected by the amplitude and duration of the voltage pulses. If the voltage-pulse duration was too long, spindle, string-jet, or spray modes appeared. When the duration was too short, no ejection was observed. A regime identification map was developed to define the ranges of amplitude and duration that yielded the micro-dripping mode, which provided a valuable guideline for designing the EHD printing process using the pulsed voltage. Many additional researches were conducted for EHD printing on developing scaling laws for the pulsed voltage to determine the pulse frequency range for a stable jetting, and developing a scaling law for determining the jetting mode for pulsation EHD printing [43-46]. A scaling law of the pulsation frequency ($f \propto (\frac{\varepsilon_0^{\ 3}}{\rho^2 \gamma})^{1/4} \frac{E^{3/2}}{d_N^{\ 3/4}}$, where ε_0, ρ, γ, E, and d_N are the permittivity of the free space, ink density, surface tension, magnitude of the electric field, and diameter of the nozzle respectively) was developed as a function of electric field and nozzle dimension, which provided valuable guidelines for process planning [46].

3. Materials and Ink Printability

3.1 Properties requirements for EHD printable inks

The electrohydrodynamic behavior imposes special requirements of the ink materials. The inks need to be in liquid-phase for EHD printing. Solutions, suspensions, and molten materials are good examples of inks that can be printed by the EHD printing process. Functional materials can be dissolved or suspended in solvents, or simply melted with temperature to prepare liquid-phase inks that can flow out of the nozzle. To achieve the required ink properties, additives (such as surfactant and humectant) are added to the ink to adjust its surface tension, viscosity, and electrical conductivity.

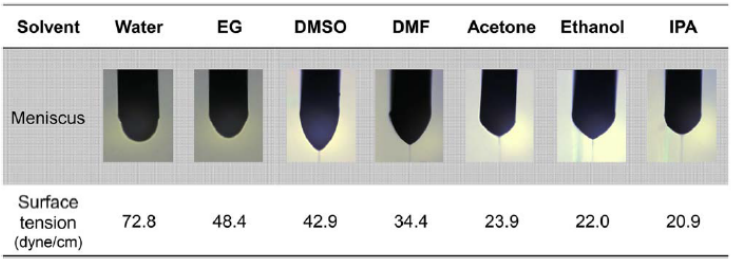

Figure 4: Effects of surface tension on proper jetting mode formation, for water, EG, DMSO, DMF, acetone, ethanol, and IPA. Reproduced with permission [54]. Copyright 2017, Wiley Publishing.

Good printability is a critical requirement for inks used in the EHD printing process. EHD printing process is not only affected by the printing conditions, such as voltage, nozzle size, and printing environment, but also the properties of the ink. These ink properties include fluidic properties (e.g. surface tension, viscosity, and density) and electric properties (e.g. conductivity and dipole moment). The proper selection of the material properties is essential for successful EHD printing [47-51]. For example, as shown in Figure 4, for materials with very large surface tension, it is very difficult to form the cone-jet and start EHD printing. Researches were conducted to find how the material properties affect the EHD printing [47-51]. The effect of the ink conductivity and viscosity on the printability of the ink was investigated in [52]. It was found that for the inks with high conductivity and high viscosity, only small Reynolds number was needed to enable the liquid flow in the cone, which makes the material printable. For inks with less conductivity and viscosity, a higher Reynolds number was needed to enable the printing process. A few systematic studies on effects of the material properties to the EHD printing performance had been performed by Bae and Yu's group [53, 54]. In those studies, materials with different viscosity, surface tension, conductivity, polymer weight concentration, relative permittivity, relaxation time were tested experimentally for their printing performance. Dimensionless numbers, such as dimensionless flow rate, dimensionless voltage, dimensionless concentration, were developed for constructing a map of the operation window for various ink materials. The results showed that the feasible jetting zone increased when the elasticity (defined as the ratio of the Zimm relaxation time to capillary time) and viscosity increased. Higher elasticity and viscosity increased the stability during the printing. On the other hand, high elasticity and viscosity reduced the printing resolution. Although not quantitative, these research results provide general guidelines for the preparation of the printable inks that can be used in the EHD printing process.

3.2 Typical functional materials for EHD printing

Broad ranges of functional materials were successfully demonstrated by EHD printing. These functional materials include nanoparticles, polymer inks that mix the polymers with solvents (e.g. water, ethanol, glycerol, acetone, etc.), biomaterials and bioagents, molten polymers and metal alloys, and 1D nanomaterials. Nanoparticles based inks are widely used for device fabrication for various printing approaches, including EHD printing. Nanoparticles of interest are dispensed in solvent to give the nanoparticle-based inks. Surfactants are generally required for such inks to avoid aggregation of the suspended nanoparticles, which can be removed through post-processing after the ink is printed onto the substrate. As one of the popularly used nanoparticles, silver nanoparticles provide many advantages, such as high conductivity, good stability, excellent thermal and optical properties, and are successfully applied in many applications such as electronics, sensors, biological devices, and photonic devices. With EHD printing, high-resolution silver conductive features were directly fabricated [55-59]. Figure 5(a) showed EHD printed high-resolution silver dot using silver nanoparticle ink. The size of the droplet was at the scale of a few microns, which demonstrated great potential for the fabrication of highly integrated electronics. The printed silver tracks were demonstrated to have a good transparency, which suits for the application of optical devices and transparent electronics. Inks with other nanoparticles, such as copper nanoparticles [60], aluminum nanoparticles and ceramic nanoparticles [61-64] were printed with high resolution by EHD printing. Micron-scale resolution was routinely obtained for these nanoparticle-based inks, as shown in the Figure 5 (a-b)).

Quantum dots are nanoparticles from semiconducting materials. Many types of quantum dot can emit light of specific frequencies if electricity or light is applied to them, and these frequencies can be precisely tuned by changing the size of the dots [65, 66]. Quantum dots are promising materials for the fabrication of advanced electronic and optoelectronic devices such as display, image detector, and solid-state lighting because of their large color tenability and narrow emission bandwidth [67]. Research from Rogers' group [68] applied EHD printing to fabricate quantum dots patterns with well-controlled resolution, registration and thickness, as shown in the Figure 5(c). These requirements on resolution, registration, and thickness were very difficult to be satisfied simultaneously by other manufacturing technologies. In EHD printing, by controlling the printing parameters such as printing speed and printing voltage, homogeneous quantum dots

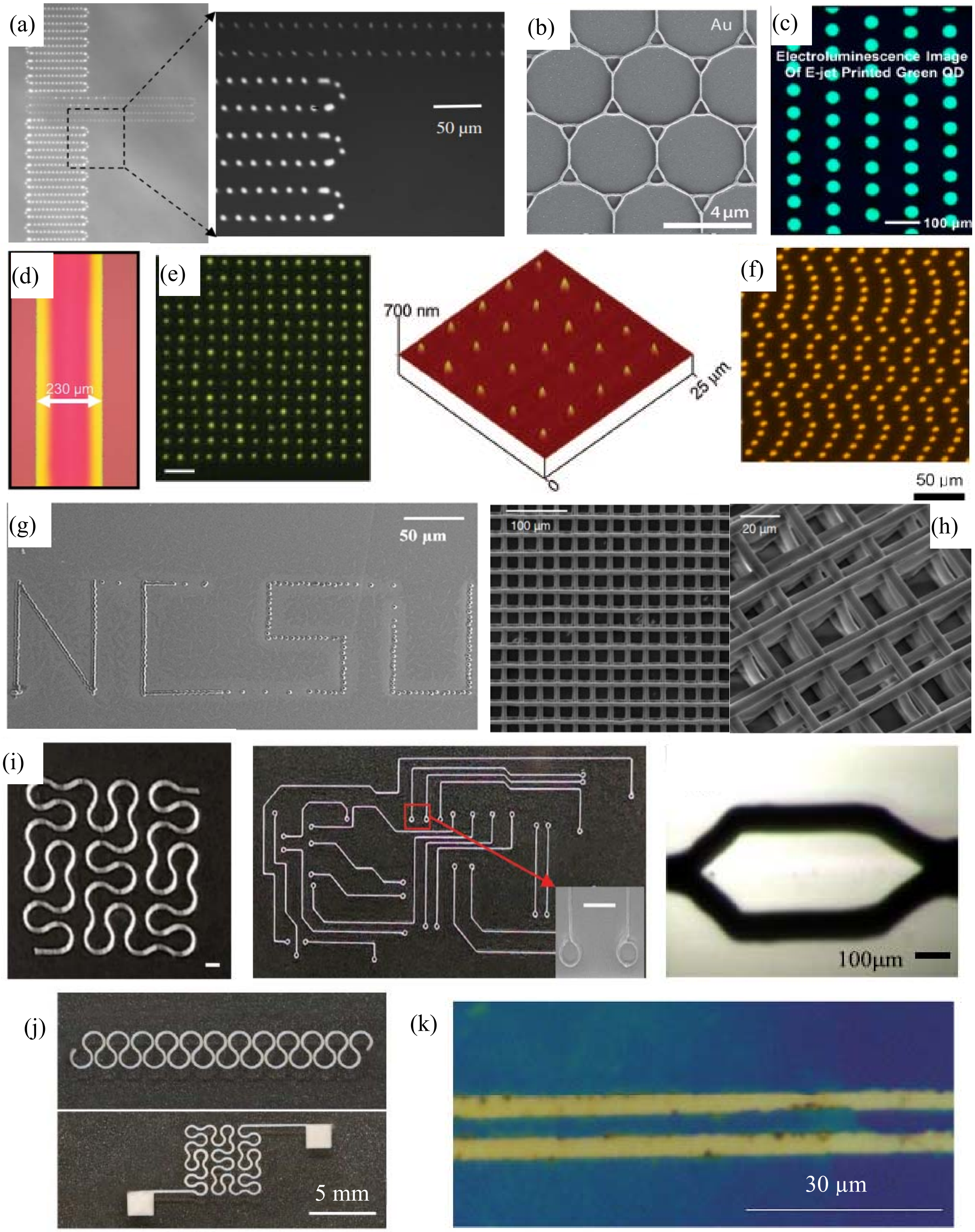

Figure 5: (a)Drop-on-demand EHD printed AgNP droplet. Reproduced with permission [58]. Copyright 2014, IOP Publishing. (b) Truncated hexagonal Au grid with a small lattice constant of 4µm. Reproduced with permission [196]. Copyright 2016, Wiley Publishing. (c) Optical micrographs of electroluminescence of green QD LEDs. Reproduced with permission [68]. Copyright 2015 American Chemical Society. (d) Printed PEDOT:PSS lines. Reproduced with permission [197]. Copyright 2016, The Royal Society of Chemistry. (e) Fluorescence micrograph (left) and AFM image (right) of printed DNA microarrays. Reproduced with permission [81]. Copyright 2008, American Chemical Society. (f) Protein microarray formed by EHD printing. Reproduced with permission [82]. Copyright 2012, American Chemical Society. (g) DoD printed wax droplet. Reproduced with permission [115]. Copyright 2014, The American Society of Mechanical Engineers. (h) EHD printed PCL scaffold. Reproduced with permission [84]. Copyright 2013, IOP Publishing. (i) EHD directly printed 2D and 3D structures using molten metal alloys. Scale bar: 500 µm. Reproduced with permission [85, 188]. Copyright 2017, Elsevier Publishing. (j) EHD printed AgNW patterns. Reproduced with permission [95]. Copyright 2018, The Royal Society of Chemistry. (k) EHD printed RGO FETs. Reproduced with permission [96]. Copyright 2015, Wiley Publishing.

patterns were directly fabricated, which demonstrated the capability of EHD printing for the direct fabrication of quantum dots based devices.

Polymer inks are also widely used materials for EHD printing due to theirs easy drying, excellent flowability, and tunable fluidic properties (e.g. surface tension, viscosity), which are used for many applications, such as biomedical scaffolds [69, 70], fabrication of nanofibers [47, 71], printing electronics [72, 73], and test materials for investigating the EHD printing process and parameters [74, 75]. Conductive polymers, such as PEDOT:PSS (Figure 5(d)), are widely used in printing electronics application [72, 73, 76-78]. EHD printing offers better resolution capabilities than other printing approaches. Polymers such as PEO solution [79] were used to investigate the mechanism EHD printing process, as their viscosity can be easily adjusted by the material concentration in the ink.

By mixing solvents with biomaterials and bioagents, such as protein and DNA, EHD printing is capable of producing high-resolution patterns of these unconventional materials, which can be used in applications of self-assembly templates [80], biosensor [81], sub-monolayer coating [82], and DNA microarray [83]. Figure 5 (e-f) shows the EHD printed high-resolution DNA and protein patterns, which have sub-100nm resolution. The applications of biological inks and the effect of the printing process to the viability of the biomaterials will be discussed in the later sections.

One specific advantage of EHD printing is its wide material adaptability. Unlike inkjet printing, which imposes quite stringent requirements on the fluidic properties of the inks (e.g. low viscous inks), EHD printing supports the fabrication of high viscous inks through the cone-jet direct writing mode. High viscous polymer melts and even molten metal alloys can be plotted with high resolution by EHD printing process [84, 85]. Figure 5(h) shows the EHD printed high-resolution bio-scaffolds using the molten polycaprolactone (PCL). PCL has very high viscosity even at the molten state (>100 kcP), but can be EHD printed into very fine filaments with sub-5um resolution [84], which is very difficult, if not at all impossible, to be achieved with traditional fabrication approaches, such as fused-deposition modeling (FDM). Metals are the other category of materials that are challenging for the printing approaches due to their viscosity and huge surface tension even at the molten state. Traditional fabrication methods for metals, such as direct writing [86-89], EBM [90], and laser sintering [91], have a very limited resolution (generally worse than 100μm). Recent works demonstrated the capability of EHD printing of low melting point metal alloys as

the printing ink. Highly uniform metallic tracks (shows in Figure 5(i)) were successfully fabricated with sub-50μm resolution, and a few 3D structures were fabricated to demonstrate its 3D printing capability [85].

The other example of the advanced material that demonstrates the great opportunity and material adaptability of EHD printing is 1D nanomaterials. 1D nanomaterials, such as nanowires and nanotubes, received significant attention with many emerging applications. For example, the random percolation network of the silver nanowires (AgNWs) showed excellent electrical, optical, and mechanical properties for applications in the next generation electronics [92, 93]. High-resolution printing of high-aspect-ratio 1D nanomaterials, especially long nanowires, which normally have their length over ten micrometers, by inkjet printing, is extremely challenging due to the risk of nozzle clogging and the difficulty to maintain the structural integrity of the nanowires through the printing process. Recent study demonstrated that high-resolution AgNW network could be printed by EHD printing approach [94]. Due to the unique printing mechanism of EHD printing, the printed jet or droplet can be a few orders of magnitude smaller than the nozzle diameter. A large nozzle can be used in EHD printing to produce micro-scale features and evade the dilemma of printing resolution and nozzle clogging. Highly alignment silver nanowires filament with sub 20μm resolution [94], and complex 2D patterns of AgNW network [95] were directly fabricated without using a mask, as shown in Figure 5(j). Recently 2D material, such as reduced graphene oxide (RGO), were also printed by EHD technology to form complex geometric devices with high resolution on both planar and highly curved surfaces [96], as shown in Figure 5 (k).

4. EHD Printing Processes and Systems

4.1 EHD printing systems

A typical EHD printing system consists a print head with a nozzle and a syringe, a pump or a pressure regulator, a power supply, a motion stage, and a control system, as shown in Figure 1[17]. The pump or pressure controlled dispensing system was used to maintain the required ink flow for the printing process. The power supply was used to apply a voltage between the nozzle and the conductive support substrate to start EHD printing and drive flow of fluid inks out of the nozzle. The motion stage that usually had a micro/nano scale resolution was moved by the control system

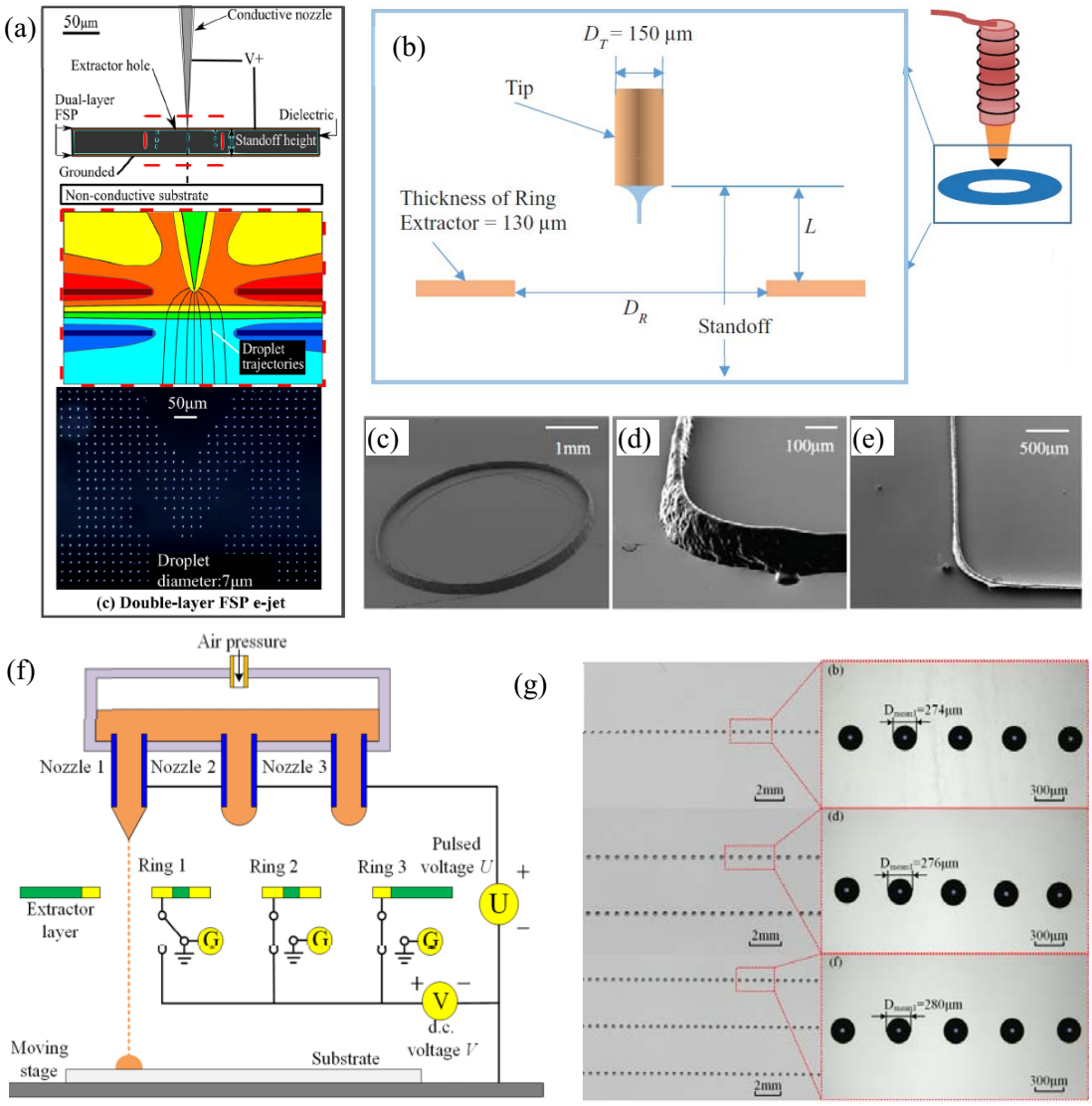

Figure 6: (a) Design concept of the double-layer FSP e-jet setup with corresponding electric field shaping, and printed patterns. Reproduced with permission [102]. Copyright 2014, American Institute of Physics. (b) Schematic of ring extractor design, and (c-e) the printed 3D micro-structures. Reproduced with permission [103]. Copyright 2017, IOP Publishing. (f) Principle scheme of the multi-nozzle multi-level voltage method (MVM), and (g) Printed droplets show good dimension consistency and position consistency. Reproduced with permission [107]. Copyright 2015, American Institute of Physics.

along the predesigned toolpath for pattern fabrication. The printing setup has the ability to print a variety of materials onto the flat substrates, and used for numerous applications.

Improvements from the traditional EHD printing system were made by many researchers to achieve better printing performance and manufacturing throughput. In the traditional printing system, the printing voltage is applied between the nozzle and the ground electrode that was placed

under the substrate. During the printing process, the standoff distance must be kept at the same level to maintain a stable printing. Such configuration limits its applications for printing on uneven substrate and printing of 3D structures. To overcome this limitation, one solution is to create a printhead that integrates the nozzle and the ground electrode together. As a result, the printing process is independent from the substrate. Gated ground electrodes with a hole in the middle were designed by a few groups [59, 97-100], which ejected the droplets or the jet through the hole onto the substrate without using the substrate as an electrode. An electric field shaping printhead capable of high-resolution (sub 10 μm) EHD printing was demonstrated using dual-layer ring electrodes [101]. In this design, two conductive plates were arranged with a dielectric material in between, as shown in the Figure 6 (a). The nozzle tip was placed at the same horizontal level with the top conductive plate, and both of them were connected to the positive voltage to focus the electric field to the center of the hole. The bottom conductive layer was connected to the ground as the ground electrode to attract the droplet or jet to the substrate. After determined the key parameters (shape and size of the hole, thickness of the plate and the dielectric material, and standoff distance) in the printing system, fine droplets with sub-10μm resolution were printed onto the non-flat substrate. With the help of airflow, similar design allowed stable printing directly on the non-conductive and tilted substrate without sacrificing the resolution [102]. Recent research from Dong's group had demonstrated the capability of applying the integrated printhead for 3D printing [103]. In their printhead design, a thin glass slide that coated with a conductive layer was set as the ground electrode, which was integrated with the printhead and located between the substrate and the nozzle. The schematic of this design is shown in the Figure 6 (b). Several key design parameters were identified and tested by the experiments. With a nozzle size of 150μm, filaments with a resolution of about 20μm were produced, and the high aspect-of-ratio (about 20) 3D structures were directly printed. The integrated printhead offered improved 3D printing capability that enabled the printing of tall 3D structures, which is very challenging by traditional EHD printing system [104]. Other improvement of the printing system on the printhead aimed to reduce the required voltage for the EHD printing. By adding a non-conductive tip to the nozzle, the voltage for EHD printing was reduced, and the printing resolution was improved [105].

The other limitation of the single nozzle based EHD printing system is its throughput. Printing multi-materials or printing with multi-nozzles allows to increase the productivity and complex of the objects, which motived many researches on the multi-nozzle system for EHD printing [106-

110]. The design of multi-nozzle for EHD printing were reported by many groups [107-110]. In these designs, the array of nozzles were fabricated by several etching processes using silicon wafer [107] or by PDMS mold [108, 109]. The distance between the two neighboring nozzles was at mm scale. Each nozzle was equipped with a separate electrode to achieve control of printing from each nozzle. Interference of electrostatic field among different nozzles are the primary preventing factor to achieve a high nozzle density and integrity. To reduce the interference, individual pumps was used to control the ink flow rate for each nozzle. The results [108, 109] showed that the stable cone-jet were observed during the multi-nozzle printing, while, using the pump to control ink flow rate of each nozzle increased the complex of the printing system. To improve the controllability of the printing process, a multi-level voltage and a multi-nozzle system were designed [107], as shown in Figure 6 (f). The designed multi-nozzle printhead for multi-level voltage control consisted of three parts: PMMA holder, stainless steel capillaries, and FR-4 extractor layer. Each nozzle was equipped with a ring extractor as a self-working isolated printhead. By controlling the voltage on each isolated printhead, the electric field strength around the apex of the nozzle can be controlled at the same level, which resulted in the identical printing behavior with the almost same droplet size and same printing frequency, as shown in Figure 6 (g). With the multi-nozzle design, high production capability was demonstrated for printing different metallic colloidal inks. Multiple micro-tracks with good conductivity were directly printed onto the substrate simultaneously, which effectively scaled up the throughput of the overall printing process [108, 109].

Multi-materials printing allows fast production and heterogeneous integration of different functionalities on a single substrate or device. Sutanto et al. developed a multimaterial EHD printing system, which allowed printing complex structures using multi-materials [18, 111]. The printing system utilized multiple individual print-heads with a carrousel indexing among them to achieve increased material flexibility of EHD printing. For the multi-material printing system, the accuracy of the nozzle position is vital for the overlay registration among features. In their design, an onboard encoder was used to measure the rotation of the printhead in macro-level, and a vision-based measurement system was selected to improve the position in micro-level and to provide feedback data on the location of the nozzles respected to the substrate. Crossover interconnects and multiple fluorescent-tagged proteins were printed onto the substrate with micron-scale resolution, demonstrating applications for printed electronics and biological sensing.

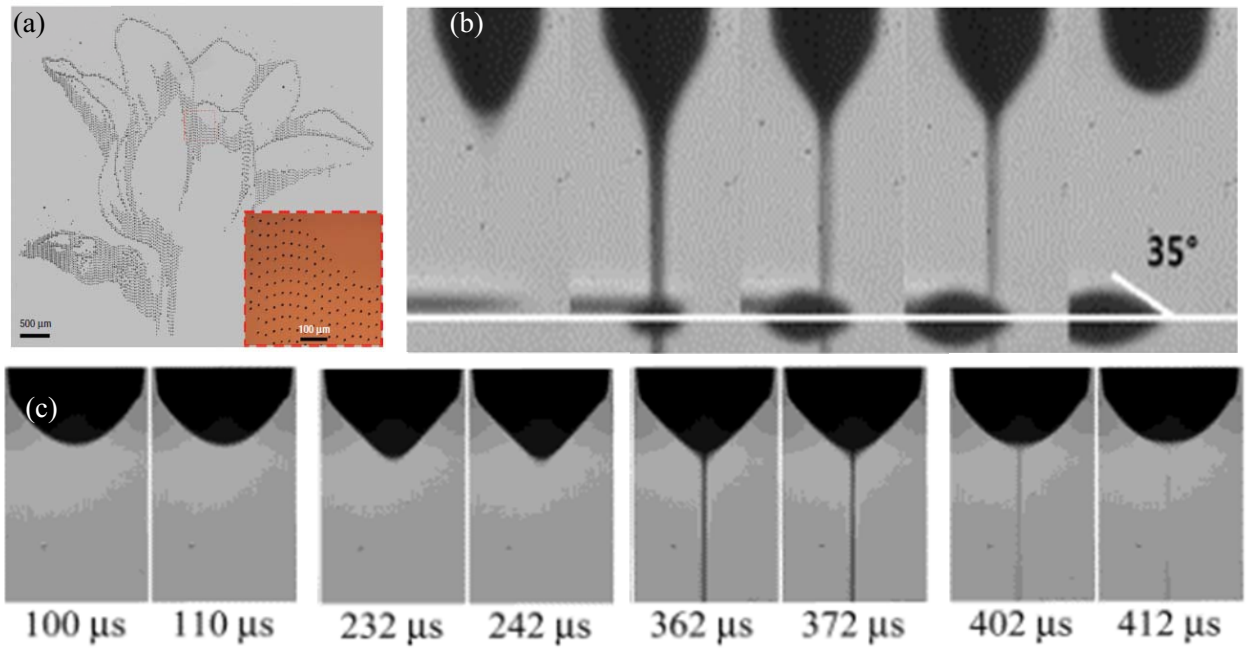

Figure 7: (a) Image of a flower pattern formed with EHD printed dots (~8 μm diameters) of SWNTs from an aqueous solution. Reproduced with permission [17]. Copyright 2007, Nature Publishing Group. (b) High speed camera image of EHD DoD printing of silver nanocolloid using pulsed voltage. Reproduced with permission [117]. Copyright 2014, Springer Publishing. (c) Time-lapse image of EHP DoD of methanol solution with a constant DC voltage. Reproduced with permission [45]. Copyright 2004. The American Chemical Society.

4.2 EHD printing processes for micro/nano manufacturing

For printing-based micro/nano manufacturing processes, the capability to precisely deliver functional materials to the designed location is critical for the high precision fabrication. Among many jetting modes of EHD printing, the micro-dripping mode (i.e. pulsating mode) and the stable cone-jet mode provide such high precision fabrication capability. In the micro-dripping mode, separate droplets are generated from the meniscus by the electrostatic force and printed onto the substrate, which provides the drop-on-demand (DoD) printing capability. Using the stable cone-jet mode, a thin jet of the ink is ejected from the Taylor cone, and a filament is deposited onto the substrate, which provide direct writing capability. Both printing modes received significant attention from the research community, and were applied in many applications.

4.2.1 EHD Drop-on-Demand (DoD) Printing Processes

In EHD DoD printing, a DC voltage is applied between the nozzle and the substrate. When the electrostatic force is large enough to overcome the surface tension force of the ink, a tiny droplet is ejected from the Taylor-cone, as shown in Figure 7. The inks used for EHD DoD printing usually

have low viscosity. A wide range of functional inks were successfully demonstrated by EHD DoD printing, such as SWNT ink [17], wax [104], silver nanoparticle ink [57], gold nanoparticle ink [112], and other conductive inks [113, 114]. Resolution ranging from tens of nanometers to tens of microns was reported, depending on different ink materials and printing configurations. In the EHD DoD printing, the size of the droplets and the ejection frequency rely heavily on the process conditions (e.g. applied voltage, flow rate or pressure) and materials properties (viscosity, surface energy, etc.). Generally, increasing the voltage will reduce the droplet size (better resolution) and increase the ejection frequency of the droplets, since a higher voltage and the resulting electric field strength increases surface charge density at the Taylor cone. As a result, droplets with smaller volume can have large enough electrostatic force to overcome surface tension to be ejected from the cone tip. The high electric field also increases the accumulation speed of the surface charge, thus the frequency of the droplet formation and ejection is increased too. On the other hand, increasing the pressure or flow rate of the ink material results in larger droplets and reduced printing frequency [17, 104, 115]. The effect of the substrate conditions on the printing performance was studied in [57]. It was found that the surface energy and surface temperature of the substrate affected the morphology of the printed droplet. The droplet on a hydrophobic surface showed a convex shape, and the droplet on a higher substrate temperature showed ring-effect.

EHD printing with a constant DC voltage is simple to use, but the controllability of the process is limited. For example, both the droplet size and printing frequency are affected by the applied voltage, which make the independent control of the droplet size and printing speed very difficult with the constant DC voltage. One solution to overcome such limitation is to control the EHD printing process using a modulated pulsed voltage. The droplets are generated by the voltage pulses, from which the pulse frequency determines the printing frequency and pulse duration determines the droplet size [42, 62, 116-122]. For a typical waveform of the modulated voltage, pulses of high voltage are superimposed over a lower baseline constant voltage [99,116], as shown in Figure 8(a). Here, the duration of the pulse and the pulse frequency can be varied, as well as the baseline and the pulse voltages. The baseline voltage needs to be carefully selected to ensure the proper operation of the process, which should be sufficiently low to not trigger printing but high enough to maintain the cone for the future droplet ejection. With this approach, the small droplets of a few microns in diameter were printed with printing frequency of 10–50 kHz.

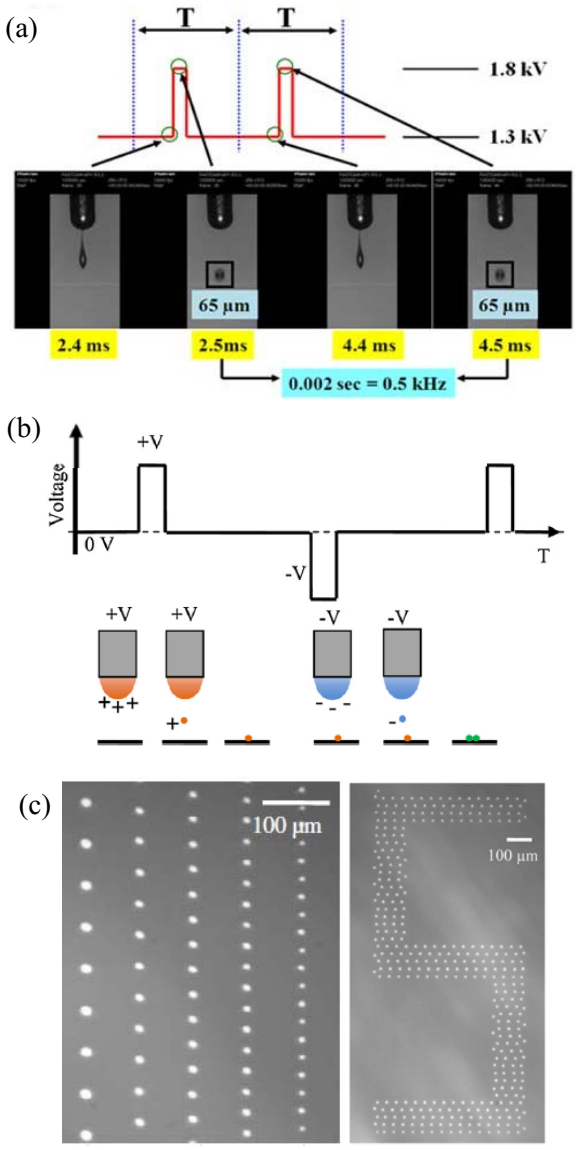

Figure 8: (a) Schematic voltage profile for the pulsed EHD printing and the resulting jetting behavior. Reproduced with permission [99]. Copyright 2008, American Institute of Physics. (b) Schematic plot of AC-pulse modulated EHD-jet printing process. Residue charge of printed droplets is neutralized on insulating substrates, and (c) drop-on-demand printed droplets with ejection frequency and droplet size controlled by parameter of the AC-pulse voltage. Reproduced with permission [58]. Copyright 2014, IOP Publishing.

Due to the specific EHD printing mechanism, the droplets ejected from EHD printing carry a certain amount of charge. A significant disadvantage of DC-based EHD printing processes comes from the build-up of the residual charges from the printed droplets, which can alter the dynamics of printing, especially on highly insulating substrates from electronic applications. As a solution to this problem, AC voltages, including AC sinusoidal voltage and AC pulsed voltage, were investigated for the EHD printing process [55, 58, 123]. When using the AC voltage, switching the polarity of the charges in the droplets periodically minimize the overall residue charge on the substrate. Figure 8(b) shows the voltage profile of AC-pulse modulated EHD-jet printing [58]. When the voltage and the pulse duration are properly selected, each positive or negative pulse can produce a droplet. The resulting printing frequency is expected to double the frequency of the pulse signal. Due to the intermittent positive and negative pulses, the charge from the consequent droplets neutralizes each other, which effectively minimize the effect of residue charge to the printing process. As the result, continuous features can be reliably printed onto the highly insulating substrates. By modulating the pulse frequency, pulse amplitude, and pulse duration, the EHD printing behavior can be controlled with respect to the printing speed and the droplet size. Printing speed

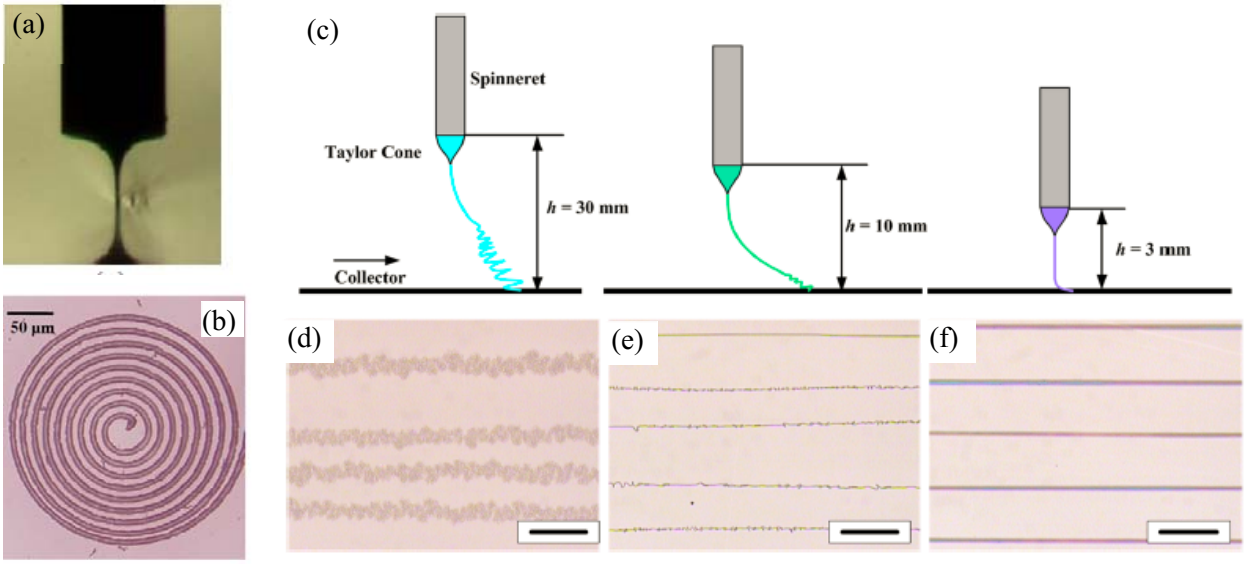

Figure 9: (a) Stable cone-jet on the EHD printing of melted PLC. (b) EHD printed circular coil pattern. Reproduced with permission [84]. Copyright 2013, IOP Publishing. (c) The deposition behavior of PEO solution jet with different standoff distance. (d-f) Plotted PEO microfibers at different standoff distance. Reproduced with permission [198]. Copyright 2016, Springer Publishing.

can be controlled by the pulse frequency, and the droplet dimension is controlled by the voltage or the duration of the pulse, as shown in Figure 8(c). Other research on controlling the EHD printing process included using various waveforms of the voltage to directly control the droplet volume during the printing [124].

4.2.2 EHD Direct Jet Writing Processes

EHD DoD printing works well for inks with relatively low viscosity. However, when the ink exhibits very high viscosity, the viscous force prevents the liquid at the apex of cone detaching from the cone as droplets, which disable drop-on-demand printing. The good news is that at proper conditions, a continuous jet can still be ejected from the Taylor cone as the cone-jet mode, and be deposited to the substrate, as shown in Figure 9 (a, b). This cone-jet mode provides direct writing capabilities using the continuous jet, and become the other promising process for micro/nano scale manufacturing. Compared with extrusion-based Fused Deposition Modeling (FDM) technology, EHD direct jet writing provides superior resolution that is vital for the high precision manufacturing. Printing voltage, printing speed, standoff distance, and nozzle size are the several important parameters of the EHD direct jet writing process [84, 125, 126]. Those parameters have to be carefully selected to achieve a stable and high-resolution printing. A relative small standard

of height is very important to minimize the whipping instability of the jet and to increase the placement precision of the ejected filament, as shown in Figure 9(c). Although the required voltage varies for different materials and different printing configurations to achieve stable printing, the general effect of the voltage on the printing process is the same. When the voltage is too low, discontinuing fibers are observed due to the limited ink flow from inadequate electrostatic force, while when the voltage is too high, the printing becomes unstable. One of the most important process conditions to achieve high quality fibers/filaments is to match the jetting speed and the printing speed, otherwise broken fibers or winding fibers may be observed, because of the mismatch between the ink flow and ink settlement on the substrate [84].

EHD direct jet writing using the stable cone-jet mode can be applied to many different materials, such as polymer solutions, polymer melts, and metal melts, despite their relatively high viscosity [69, 85, 127-129]. Moreover, EHD direct jet writing provides a promising solution for the high resolution patterning of relatively fragile 1D nanomaterials, because the jet carries 1D nano-materials through the liquid stream without excessive bending of the materials, thus maintain the integrity of the 1D nanomaterials, while the formation of micro-scale droplets in the DoD printing often breaks the 1D nanostructures. Aligned and interconnected AgNW networks were successfully demonstrated by the EHD direct jet writing process [94, 95]. Experiments were also performed to directly print conductive metal inks onto the curve surface using the EHD direct jet writing process. A small mesh electrode with high uniformity and good sheet conductivity was successfully fabricated, which can be applied for the fabrication of transparent devices [130]. By integrating EHD direct jet printing and FDM technology for thermoplastic polymers, tissue engineering scaffolds having hierarchical structures with both macro-scale and micro-scale features were directly fabricated [131, 132], which provide great potentials for advanced biomedical functions. For tissue engineering scaffolds, while the relatively large structures and pores (generally >100 um) are important for providing mechanical support and material transportation, micro-scale structures with their dimension similar to the size of the cell provide many advanced capabilities to regulate cell responses to the scaffold, such as cell alignment and cell guidance.

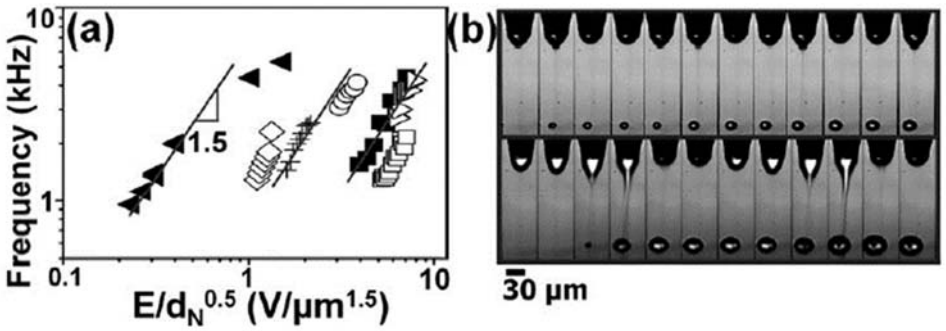

Figure 10: (a) Scaling law shows the relationship between pulsation frequency and the scaled electric field. The slop of the data in this log-log plot is approximately ~1.5. (b) Images captured using a high-speed camera for these experiments to validate the scaling law. The time separation between adjacent images is 100 μs. Reproduced with permission [46]. Copyright 2008, American Institute of Physics.

5. Theoretical and Numerical Modeling of EHD Printing Processes

It is critically important to understand the mechanisms of the EHD printing process and model the relationship between the printing parameters and the printing results, so as to plan and optimize the printing process to achieve the best performance. Many analysis and models were investigated to correlate the process conditions with the resulting printing behaviors, such as the printing mode, the droplet/jet size, and the printing frequency.

Theoretically modeling the electrohydrodynamic behavior is very challenging due to its coupled multi-physics. Hartman and et al. investigated theoretical models and simulation tools to study the cone-jet mode [39]. In their study, an analytical model was developed to calculate the shape of the liquid cone and jet, the electric fields in and outside the cone, and the surface charge density at the liquid surface. The results of the cone-shape model fitted well with experimental values. Moreover, physical equations and both analytical and numerical models were derived to predict the droplet size for one main droplet and a secondary droplet, charges on the droplet, the break-up velocity of the droplet, and the wavelength of the break-up. Models for the jet break-up in cone-jet mode were further developed with experimental verification using high-resolution camera and long-distance microscopic lens to verify the simulation results. These models provided good understanding of the mechanism for the cone-jet mode in EHD printing, and suggested scale law between the droplet diameter and the flow rate [39-41].

Based on the theoretical analysis of the electrohydrodynamic behavior, a few scaling laws were developed for the EHD printing at the pulsating mode and cone-jet mode [46, 133]. These scaling

laws indicated that the jet size is proportional to the square root of the nozzle diameter, but inversely proportional to the electric field intensity. The pulsation frequency is proportional to the 1.5 times of the electric field intensity that show in the Figure 10. The scaling laws provided valuable insights on the general effect of different process parameters (e.g. voltage, flow rate, nozzle size) on the printing output (e.g. jet size and frequency). Although the scaling laws do not directly provide the quantitative values of the process parameters for achieving the desired printing results, they give valuable guidelines and directions for the process improvement and process optimization.

Due to the complexity of the theoretical modeling approach, numerical methods, including Finite Element Analysis (FEA) methods, were widely used tools to study the mechanism of the EHD printing process. The whole EHD printing process can be divided into a few stages, from the cone formation, droplet ejection, droplet in-flight, and droplet impact/settlement on the substrate. Numerical modes were developed for these different printing stages. A FEA model was developed for droplet breakup at the end of the cone by integrating two-phase flow, electrostatics, and charged species transport together, which can simulate the droplet size, charge and mass of the droplet [134]. The surface property of the nozzle also affected the cone formation at the nozzle tip. A model was created to study the liquid cone around the nozzle with hydrophobic and hydrophilic surfaces, and it was found that the hydrophilic nozzle required less electric field strength for droplet ejection [135]. Once a droplet was detached from the cone, its flight behavior was affected by the charge on the droplet and the accumulative charge on the substrate, which was studied by a model in [136]. A set of FEA models were developed by Dong' group [74, 115] to predict the EHD printing behavior from the droplet formation to droplet settlement for the drop-on-demand EHD printing. The droplet size, inflight velocity, and final droplet footprint and height on the substrate were successfully predicted from the model [74, 115]. The droplet formation in EHD printing was modeled by FEA, as shown in Figure 11 (a). Two important forces in EHD printing, electrostatic force and surface tension force, were modeled separately by Finite Element Analysis. The droplet size was obtained by balancing the electrostatic force and surface tension of the pending droplets around the meniscus apex. The force-balance based FEA model was capable of predicting the diameter of the ejected droplets with good accuracy with the maximum error of model prediction less than 10%. This simulation provided a good insight for understanding the mechanisms of the EHD printing, and provided guidelines for EHD printing process design. However, in this

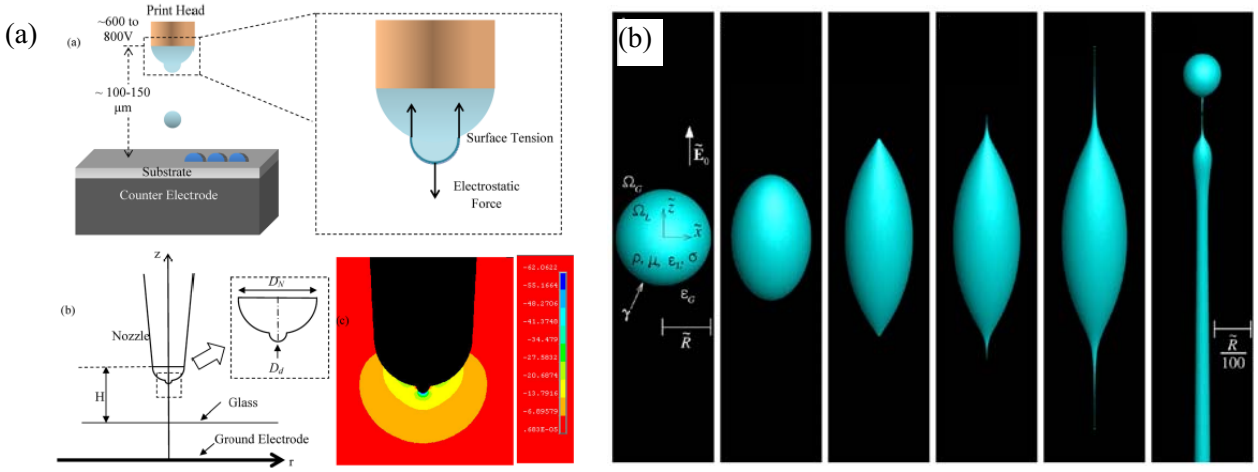

Figure 11: (a) Schematic configuration for FEA modeling of the electrostatic force on the droplet and the electrical field distribution around the nozzle tip during the droplet ejection. Reproduced with permission [115]. Copyright 2014, The American Society of Mechanical Engineers. (b) The change of the tip-streaming from an uncharged, slightly conducting liquid drop subject to a uniform external electric field. Reproduced with permission [141]. Copyright 2013, National Academy of Science

simplified model, only surface tension property of the ink was considered during the simulation. Collins et al. developed both theoretical models and numerical simulation models to study the EHD jet formation and jetting mode [137]. In their work, an axisymmetric G/FEM three-dimension algorithm was developed to study the dynamic response of a highly conductive incompressible Newtonian jet under the electric field. Using the axisymmetric model, the algorithm can provide an accurate description of the dynamic evolution of jet formation, jet breakup, and droplet pinch-off, as shown in Figure 11(b), which are difficult to measure and visualize experimentally. Despite many progresses of using FEA to study different aspects of the EHD printing process, developing a comprehensive model that can integrate the critical ink properties (e.g. surface tension, viscosity, and conductivity) for multiphase droplet/filament simulation remains an important topic that needs further investigation. It is still very challenging to build a comprehensive multi-physics model to simulate the overall EHD printing process due to its large complexity and coupled physics. Fully modeling the relationship among the material properties of the inks, the printing conditions, and the resulting printing behaviors will be beneficial to better understand and utilize the EHD printing process.

Numerical method is a powerful tool to simulate and understand the different aspects of the EHD printing processes [40, 51, 138-140]. Several studies applied the numerical method to study

the droplet size and the charge of the droplet during the EHD printing. It was found that the droplet size and the charge of the droplet were determined by the ink conductivity and three scaling regimes defined by viscous time. The charge of the droplet determines if the process could keep the stable condition. When the charge was below Rayleigh limit, the process would become unstable [141]. Modeling the cone-shape during the EHD printing helps to understand the printing process. An axis-symmetric equation of continuity, electric potential and momentum was used to describe the cone shape in the cone-jet mode, which gave useful information on the electrically driven jets [142]. Numerical model was also used to study the droplet-substrate interaction [143]. A spherical cap volume conservation law and molecular kinetic were used to simulate the droplet spreading on the substrate. The simulation result gave a good agreement with the experimental result [143]. The volume of Fluid (VOF) method with multiphase flows was used recently to study the EHD printing process [32, 33, 144]. Reynolds, Electro-Weber and Weber number were used to reduce the computational load. These numerical studies can predict the jet diameter under different material properties. Numerical study for EHD printing using AC and pulsed voltage were also studies by a few groups [145, 146] to predict the droplet size under the pulse voltage, and to find the optimal signal that can be implemented to the EHD printing process. The simulation results showed a good agreement with the experimental results.

6. Applications of EHD Printing

6.1 Additive Manufacturing

Additive manufacturing, as a fast-growing technology, enables rapid prototyping or free form production of complex components for automotive, aerospace, medical, and electronic applications [147-150]. High-resolution additive manufacturing is critical for many emerging applications. Many high-precision industrial parts require micron-scale accuracy and high-quality surface finish. A high-resolution additive manufacturing process can possibly satisfy such specification and produce the parts directly, which may effectively reduce the time and cost in post-processing. In biomedical applications, such as tissue engineering scaffolds, micron-scale structures that have their dimension like the size of the cells, can be directly used to regulate cell responses by contact guidance. Most of the existing additive processes, including 3D printing, stereolithography, selective laser sintering, electron beam melting, and fused deposition modeling

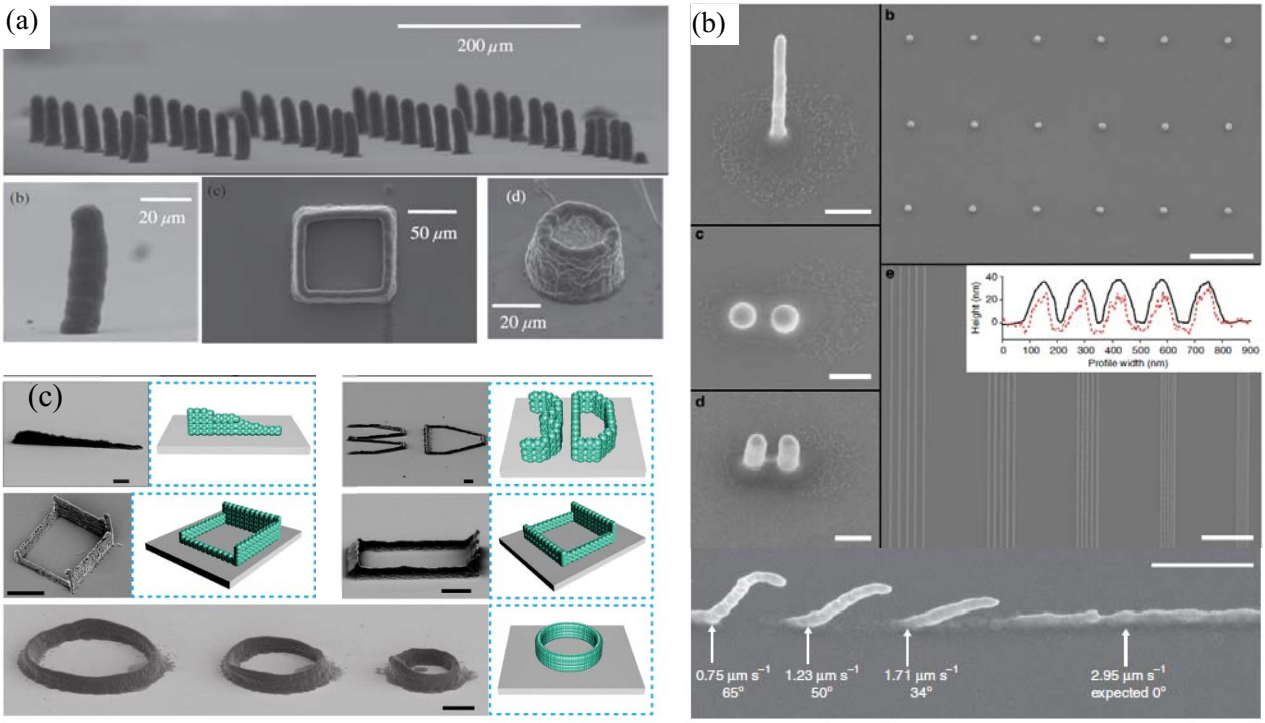

Figure 12: (a) Electrohydrodynamic 3D printing using a phase change material (wax) as the ink. Reproduced with permission [104]. Copyright 2014, Elsevier Publishing. (b) Direct printing of silver pillars by auto-focusing EHD printing. Reproduced with permission [112]. Copyright 2012, Nature Publishing Group. (c) Schematic and SEM images of 3D wall structures made of anthracene and TIPS-pentacene. Reproduced with permission [152]. Copyright 2015, Wiley Publishing.

[151], generally have their best resolution no better than 50μm. The resolution limitations from the existing processes are intrinsic and difficult to overcome.

EHD printing provides high resolution alternatives for a few existing printing processes that were widely used in additive manufacturing. More specifically, EHD drop-on-demand printing has the similar operation principle to the inkjet printing that is the basic process in 3D printing, while EHD printing can offer much smaller droplet sizes than the inkjet printing. EHD direct jet writing is analogous to the extrusion processes, such as those used in fused deposition modeling, but again offers significantly better resolution for the printed filaments. As a result, EHD printing represents a set of new processes with promising potential for 3D printing that can printing 3D structures with micro-scale resolution. So far, most of the EHD printing applications focused on the fabrication of two-dimensional (2D) patterns with low aspect ratios and limited three dimensionality. Only a few initial investigations demonstrated the capability of the EHD printing towards 3D fabrication. Recent work by Dong and co-workers [74, 104, 115] demonstrate high-

resolution 3D printing using the EHD drop-on-demand printing process. 3D objects were successfully fabricated with critical dimensions smaller than 10 um and aspect ratios as large as about 8, as shown in Figure 12(a). In their study, a phase-change ink, paraffin wax, was used as the printing material, which was melted in the syringe as the ink and solidified quickly by the temperature gradient after printed from the nozzle, enabling build the 3D structure layer by layer. Since wax was already widely used as the modeling and supporting material for additive manufacturing, this work directly demonstrated the applicability of EHD printing for the additive manufacturing applications. Besides phase-change inks, other functional materials were also demonstrated recently by EHD DoD printing. Galliker et al. successfully fabricated out-of-plane vertical pillars and titled pillars by EHD printing using an auto-focusing effect [112], as shown in Figure 12 (b). The used fast-vaporization ink was able to carry away the charge from ink vaporization, for which the charge relaxation time was less than the droplet ejection time. The printed nano-bump acted as a sharp electrode that attracted the follow-on droplets because of the electrostatic field-focusing effect, to fabricate high aspect ratio pillars with 50-nm width and 850-nm height. Park el al. [152] applied EHD printing to fabricate 3D features of diverse materials, including organic light-emitting small molecules and metallic or magnetic nanoparticles, with relatively complex shapes (e.g., arrays of pillars with high aspect ratios, walls, helical structures, and arch-like bridges) and with resolutions into the submicrometer scale, as shown in Figure 12(c). Multi-material integration capability in three dimensions by EHD printing was also demonstrated for the vertical assembly of 3D patterns of heterogeneous materials [152]. EHD direct jet printing represents the other approach for 3D printing. Using thermoplastic polymers, such as polycaprolactone (PCL), EHD direct jet printing can eject microfilament from the molten polymers for the fabrication of 3D porous scaffolds [131, 132, 153], as shown in Figure 5(h).

Despite all the advantages and initial success offered by EHD 3D printing, a few challenges from the EHD printing processes need further investigation to make EHD printing technically feasible and commercially competitive for the additive manufacturing industry. One challenge in EHD printing is its low throughput, which is partly a side effect of its high-resolution capability. Due to the small droplet produced from EHD printing, it will take much longer to produce an object with a given volume. EHD printing using multiple nozzles, as discussed in section 4.1 represents a possible solution to enhance the printing efficiency. The other potential pathway to increase the printing productivity is hybrid printing that integrates conventional printing and EHD

printing, in which conventional printing is used for the high volumetric production of the main structures of the object and EHD printing is applied for the fabrication of the high-resolution features and structures. The other challenge of the EHD-based 3D printing process is the limited height that can be printed by the EHD printing system and process. In the traditional EHD printing setup, the ground electrode is placed with the substrate, which has limited capability for 3D manufacturing. As 3D structures are built up layer-by-layer, the nozzle-substrate gap has to be changed accordingly. It is very challenging for process control to keep the constant electric field strength. Moreover, if tall structures need to be printed, the resulting large nozzle-substrate gap may require a voltage that is too large to be provided. On the other hand, since the dielectric constants of the printing materials are usually different from that of air, electric field strength and field distribution could be affected and complicated by the printed features on the substrate, and the future printing behaviors could be difficult to predict, which further increase the difficulty in reliable process control. Integrating the ground electrode to the printing nozzle, as discussed in section 4.1, helps to relieve this challenge by effectively increase the maximum structure height that can be printed. More research efforts on the process development, new printing systems, and process control are required to overcome the technical barriers to make EHD printing a commercially competitive process for the future additive manufacturing industry.

6.2 Biomanufacturing and Healthcare

EHD printing has great potential for biomanufacturing and healthcare applications [154-159], in which high-resolution patterning of biomaterials, bio-agents, biomolecules, and even living cells is often required. These materials are very sensitive to other chemicals and environmental conditions, which limit the available fabrication approaches for them. For example, conventional lithographic methods are generally unsuitable for such sensitive biomaterials, due to the destructive radiation and toxic chemicals (photoresist as an example) from the process. Printing turns out to be one of the effective process that can pattern such materials safely onto a substrate.

Bioprinting allows patterning many different biomolecules and even constructing tissue or organs piece by piece from living cells. Cell based bio-ink can be printed at the predefined locations accurately, which bring a wide range of applications, such as *in vitro* testing of pharmacological molecules with faster response and reduced load on animal testing [160]. Many studies were conducted on the bioprinting of bio-inks [161, 162], but a high-throughput, high-

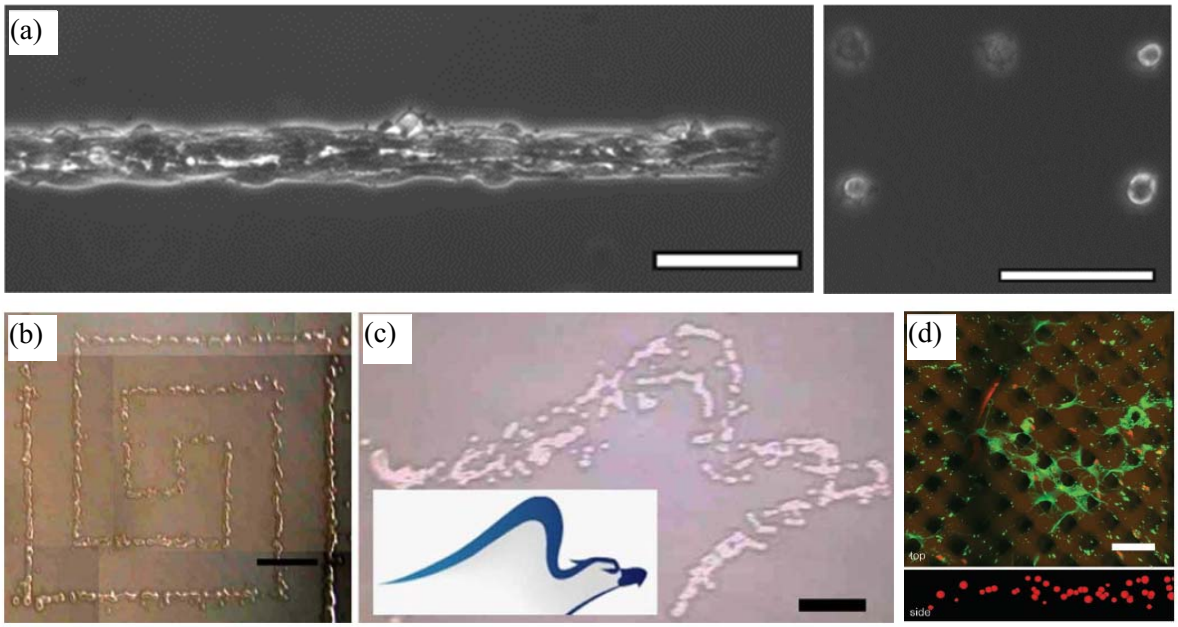

Figure 13: (a) EHD printed densely packed D15 on a narrow rectangle of patterned fibronectin and the printed spot which is small enough to constrain single cells. Scale bar: 50μm. Reproduced with permission [164]. Copyright 2011, Wiley Publishing. (b) EHD printed spiral rectangular shape of the bacterial colony pattern. (c) bacterial pattern of the eagle. Scale bar: 2mm. Reproduced with permission. [159]. Copyright 2009, Springer Publishing. (d) Confocal images of primary rat hippocampal cells distributed within scaffold, primary monoclonal antibody for actin is used to label the processes (green), while TO-PRO3 was used to label nuclei (red). Reproduced with permission [199]. Copyright 2011, Wiley Publishing.

resolution and high load printing method is still missing. EHD bioprinting allows high-precision control of mass deposition to the designated location, which becomes very important requirements for bioengineering. Hydrogel is a widely used biocompatible material and was demonstrated as one of a suitable material for EHD printing [163, 164], as shown in Figure 13(a). The ink that mixed hydrogel with cells allowed the cell to survive during and after the printing. Researchers have already used EHD printing to produce the cell-laden device/scaffold that can sustain cell survival [155, 160, 165]. Multiple studies have investigated the effect of the EHD printing on the cell viability, proliferation, and ability to grow in 3D structure [166]. Human cells mixed with 2% alginate was used as the printing ink, and a confocal microscopy and DNA quantification assays were used to characterize the printed features. The results showed that the EHD printing only had a mild effect on the viability of the cells, and the cells fully recovered to the normal proliferation rate in a week [166]. Bacterial cells were also demonstrated to be EHD printable on a membrane filter and a culturing plate, as shown in Figure 13(b,c) [159], which has the potential for

pharmacological screening of drug effectiveness and toxicity [167]. Shigeta et al. reported the fabrication of micro/nano protein patterns with EHD printing on different substrates, ranging from flat silica substrates to structured plasmonic crystals, suitable for micro/nanoarray analysis and other applications in both fluorescent and plasmonic detection modes [82]. The result showed that the EHD printing can print diverse classes of proteins over a large area and revealed that the high voltage in the EHD printing process did not adversely alter the protein structures or biological functions, which demonstrated a strong potential of EHD printing for opportunities in the printing of advanced protein microarrays for numerous applications in biology and medicine [82]. EHD printing was also successfully applied to produce DNA microarray that is widely used in biotechnology due to the rapid identification of gene expression [81]. The key parameter for measuring the DNA microarray is the number of dots per unit area. EHD printing allows printing highly compact matrix of submicron size DNA droplets. After characterization, the experimental studies showed that the DNA dots were not affected by the EHD printing process and this EHD technology has great potential to be applied for the fabrication of biosensor, nanoelectronics, and other fields [81].

Biomedical polymers were applied for EHD printing to fabricate biocompatible composites or structures [158, 168, 169]. Biomedical scaffolds are the key components to support cell attachment, growth, proliferation and differentiation for tissue engineering functions. The porosity and pore size are the key parameters when evaluating a scaffold design. Traditional scaffold fabrication methods cannot provide high-resolution pore size and micro-scale structure, and the produced scaffolds lack of repeatability for the distribution of the pores [170]. Recent research has demonstrated that scaffolds with small pore size and uniform pore distribution can be fabricated by the EHD printing approach [69, 84, 127, 171-175]. Figure 13 (d) shows cell distribution in the 3D hydrogel micro-periodic scaffold with well controlled pore size, which shows excellent cell response and interaction in the scaffold. Research from Hwang's group developed a motionless EHD printing process for bio-degradable polymer to produce a pattern with the capability of controlling the performance of drug deliver and drug release [176].

6.3 Fabrication of Electronic devices

Fabrication of electronic devices is one of the top applications for EHD printing [177-182]. Compared with traditional electronic manufacturing approaches that utilize lithographic patterning,

physical or chemical vapor deposition of functional materials, and dry/wet etching to define device features, printing processes offer many unique advantages for the fabrication of electronics. As additive fabrication approaches, printing processes directly deliver functional materials onto the substrate to produce devices directly from the design without using a mask, which enable low-cost rapid-production of customized electronic devices. Moreover, printing technology has unique capabilities to deliver a wide range of functional materials that may not be compatible with semiconductor manufacturing processes onto unconventional substrates, such as flexible/stretchable substrates and uneven curved surfaces. As a result, printed electronics became an emerging industry and received significant attention from electronics manufacturing community. Although ink-jet printing is currently an industrial standard for printed electronics, as the technology is widely accessible for a few decades, it is now lagging behind the demanding resolution requirements from the fast-evolving electronic industry. The state-of-art electronics keep pursuing higher level of feature/function integration and reduction of critical feature sizes to achieve better performance, such as enhanced functionality, fast speed, less power consumption, etc. EHD printing, as a high-resolution printing approach, satisfies such demanding resolution requirements for future printed electronics.

EHD printing has already been demonstrated as an effective method in electronics fabrication, with many electric devices successfully fabricated. Several researches applied the EHD printing process to fabricate sensors such as touch sensor [183], microcantilever sensors [184], and strain sensor [72]. The flexible touch sensor was directly printed by EHD printing onto a flexible substrate (PET) with carefully controlled plotting speed and printing voltage. The conductive material used for the fabrication of the touch sensor was silver nanoparticles with the weight ratio of the nanoparticle about 20 -35%. The printed touch sensor exhibits good flexibility and sensitive response to the touch signal [183]. Microcantilever sensor can provide highly sensitive label-free detection of various analytes. With EHD printing, the polymer droplets with diameter less than 10μm were successfully deposited to the tip of the cantilever [184]. The precise printing capability for the deposition of polymer functional layers onto microcantilever sensors with micrometer resolution provides a promising approach to functionalize the sensors to detect more analytes with higher sensitivity. PEDOT:PSS is a transparent, conductive polymers, which is highly stretchable and ductile. Mix PEDOT:PSS with PVP, Nafion, and NMP, the micron strain sensor was directly

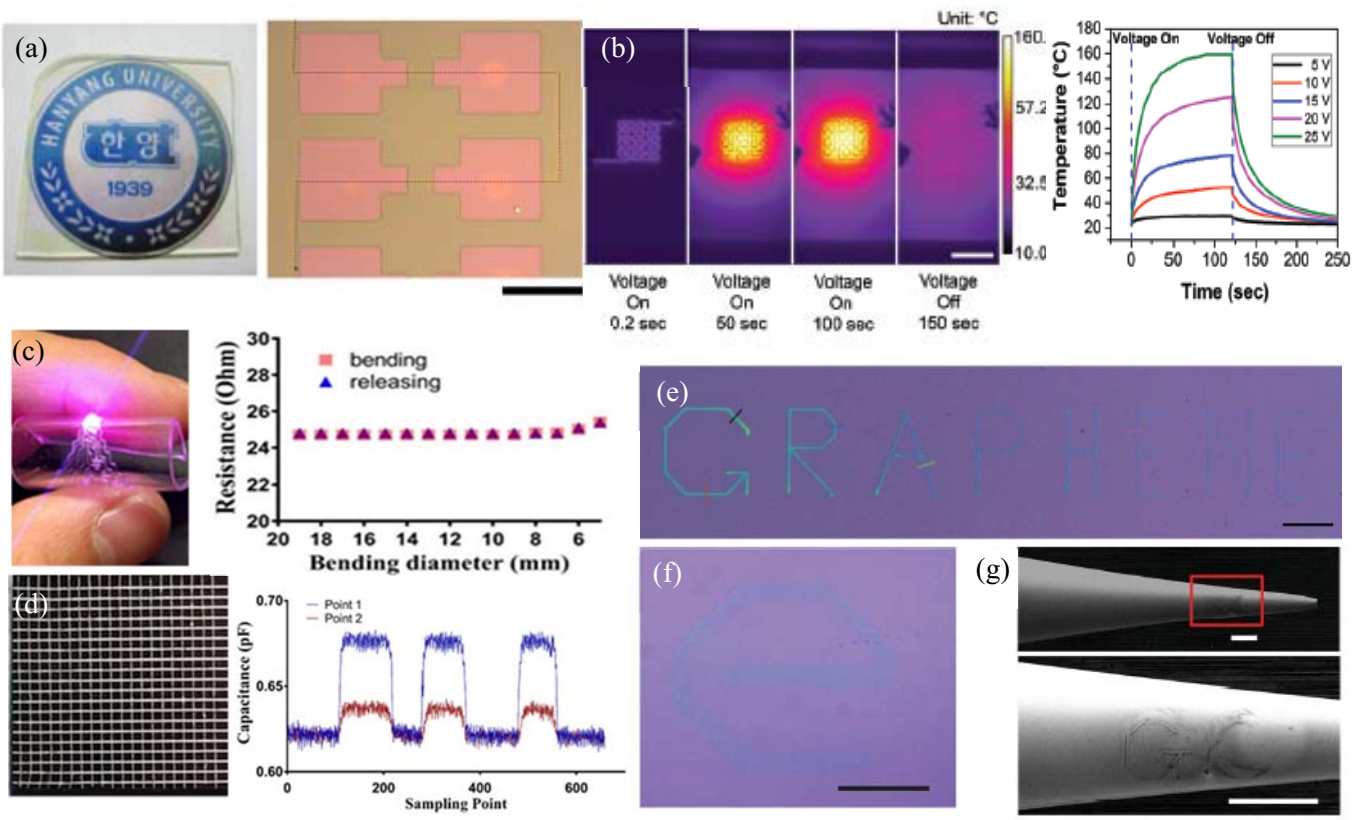

Figure 14: (a) Transparent thin film transistors with EHD printed semiconductors. Scale bar:300µm. Reproduced with permission [185]. Copyright 2012, American Institute of Physics. (b) Printed AgNW heaters and time response of the AgNW heater (scale bar, 5 mm). Reproduced with permission [95]. Copyright 2018, the Royal Society of Chemistry. (c) EHD printed conductor on PDMS, A stable electrical response was achieved during bending test. (d) EHD printed 20 x 20 matrix of touch sensors over a 10x10 mm area, the touch signal from each individual sensor was detected by the change in the capacitance. Reproduced with permission [188]. Copyright 2018, Wiley Publishing. (e) EHD printed reduced graphene oxide (RGO) with different thickness. Scale bar: 200µm. (f) High-resolution printing of (RGO) on nonplanar surfaces. Scale bar: 50 µm. (g) SEM images of the RGO patterns printed on the sidewall of a glass microcapillary as the substrate. Scale bars: 100 µm. (e-g) Reproduced with permission [96]. Copyright 2015, Wiley Publishing.

printed [72]. A bending-induced strain test was performed for the printed sensor and the result showed the printed sensors had a sensitivity of 0.06mm^{-1} to the applied stain.

Transistor is a key component in electronics. EHD printing was successfully applied to fabricate a transparent thin film transistor by Lee et al. [185], as shown in Figure 14(a). EHD printing methods offered a high level of resolution (about 1.5 µm) that provided a pathway to printed transistors with small critical dimensions. As the results of the high-resolution features, the field effect mobilities of 32 cm^{2}V^{-1}S^{-1} with an on/off current ratio of 10^3 was achieved [185]. Using EHD printing, a high-resolution reduced graphene oxide (RGO) transistor was successfully

fabricated over a large area with the feature size about 5μm [96]. EHD printing provided not only high resolution, but also good control over the feature thickness, as shown in Figure 14(e). Besides printing on the flat surface, the ability of printing on the curve surface was demonstrated (Figure 14(f)), which can be further applied for 3D printing. Figure 14(g) shows the reduced graphene oxide patterns that were even printed on the sidewall of a glass microcapillary as the substrate [96]. The other research on the EHD printing of electronics includes print photo-reactive spacers for liquid crystal display (LCD) to substitute traditional spacers [186].

EHD printing can pattern many functional materials for advanced electric application, such as flexible and stretchable electronics [187]. One dimensional silver nanowires, which is very difficult to be printed due to its large length, can be printed into the high-resolution AgNW network by the EHD printing approach. The printed AgNW conductor demonstrated excellent flexibility and stretchability. The resistance of the printed conductor kept constant during 200 times of bending and only changed slightly after 300 times of stretching, and the resistance kept a constant value when the applied strain was up to 30%. A wearable heater with complex geometric design was printed onto a lab-use glove, as shown in Figure 14(b). A uniform heating performance was observed, indicating good uniformity of the printed features [95]. EHD printing was also utilized to print low melting point metal alloy for flexible and stretchable electronics with self-healing capability [188]. With properly designed 2D patterns, the printed conductors demonstrated excellent flexibility and stretchability. A stable electrical response was achieved after hundreds of bending cycles and during stretching/releasing cycles in a large range of tensile strain (0–70%), as shown in Figure 14(c). Due to the low melting point of the metal alloy ink, the printed conductor demonstrated self-healing capability that recovered from failure simply by heating the device above the eutectic temperature of the metal ink and applying slight pressure. With high-resolution patterning capability from EHD printing, a high-density touch sensor array (20 x 20 matrix or 400 touch sensors on a 10x10 mm area) was successfully fabricated, as shown in Figure 14(d), and touch signal from each individual sensor was detected [188]. Electrodes and interconnects are some other important components for electronics. Silver or gold nanoparticles are the two primary materials for the electrode fabrication [126, 130, 189]. Byun and et al. developed an EHD printing process to fabricated invisible metal-grid transparent electrode [189]. The metal trace with linewidth of less than 10μm was fabricated. Different gaps of the trace were tested for the transparency of the fabricated patterns. With a gap of 150μm, the printed pattern showed the best

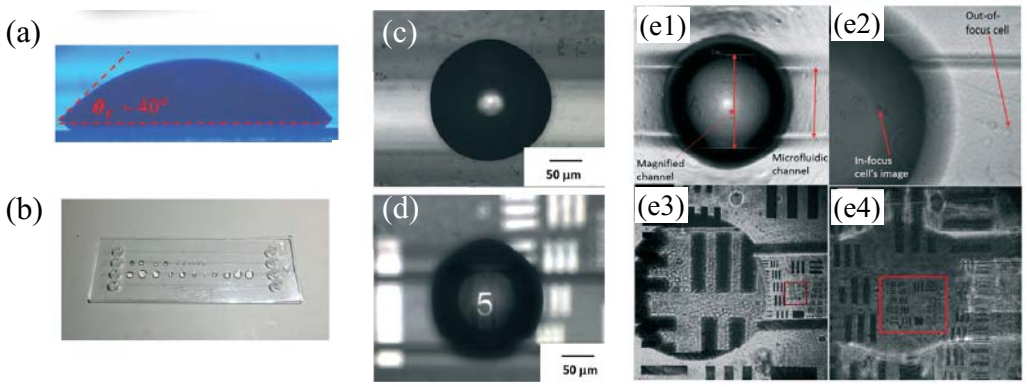

Figure 15: (a) Cross-sectional view of polymer microlens on a surface after treatment using Fluorolink S10 providing a hydrophobic condition. (b) Representative image of a thin fluorinated layer onto a microfluidic chip with printed and cured lenses formed with different diameters of 150–1500 µm. (c) Optical microscope images of the polymer microlens on the microfluidic chip. (d) The polymeric microlens was positioned over the USAF target and observed under an optical microscope. (e1-e4) Microlenses were directly deposited on-board chip. Reproduced with permission [193]. Copyright 2016, The Royal Society of Chemistry.

performance in resistance and transmittance, which are 4.87Ωsq^{-1} and 81.75%. Compared with the metal trace by inkjet printing. EHD printed electrodes was invisible due to the small line width from its high-resolution printing capability. Further research also demonstrated good flexibility of the printed electrode, whose resistance only changed for less than 20% after 500 times of bending [55].

6.4 Fabrication of optical devices

Optical devices generally have stringent requirements on the size and tolerance of the manufactured structures. So far, among most of the existing printing approaches, EHD printing provides high patterning resolution and becomes a promising candidate for the fabrication of optical devices, such as microlens, waveguides, and light-emitting diodes (LEDs) [68, 190-192]. Yudistira's group demonstrated using metamaterials for EHD printing with a resolution of a few micrometers [190]. A pulse voltage was used to control the DoD printing process, and the printed features had a high refractive index with a peak value of refractive index of 18.4 and frequency of about 0.48THz. EHD printing was successfully applied to print microlens from PDMS [193], as shown in Figure 15. High viscosity polymers (e.g. PDMS) can be easily manipulated for the optical functionalization of lab-on-a-chip devices. The PDMS liquid droplets were directly deposited onto microfluidic chips and optical fiber terminations to provide advanced optical functions. Sutanto

and et al. fabricated a few optical devices including a microlens array, an optical waveguide multiplexer, and a multi-refractive index diffraction grating using EHD printing of UV curable glue, which is widely used material in the optical systems [192].

Quantum dots (QD) are semiconducting nanoparticles, which can emit light of specific frequencies when excited by electricity or light. Quantum dots have been widely used for the fabrication of advanced optoelectronic devices such as light-emitting diodes. EHD printing was utilized by researchers to fabricate high-resolution QD patterns [68, 191]. With EHD printing, quantum-dots features with resolution about a few nanometers were deposited on both flat and structured substrates [191]. It was demonstrated that the EHD printing method can precisely control the dots at plasmonic hot spots, which can provide arbitrary wavelength, shape, and intensity. Kim et al., [68] applied EHD printing to achieve high-resolution patterns of QDs for the fabrication of light emitting diodes (LEDs). The resolution of a few hundred nanometers was successfully achieved for such QD patterns. The LEDs using printed QD films demonstrated better maximum luminance and external quantum efficiency than those from similar devices fabricated by traditional deposition techniques.

6.5 Self-assembly of Nanomaterials

Self-assembly is an emerging technology that has attracted many attentions in recent years. Self-assembly of block-copolymers have many applications for the fabrication of nano-devices [80, 194]. Self-assembly has critical requirements on the orientation of the printed features, which is also difficult for traditional manufacturing method to produce. For example, it is difficult for the current film deposition technology to fabricate the thin film with controlled geometry and size at the desired location. Onses' studies [80, 194] has shown that EHD printing could print self-assembly pattern ranging from centimeter scale to 10nm scale. The BCPs with multiple MWs and compositions can be printed onto the same substrate, which has the potential for providing multiple geometry changes and functions. The printed ink consisted of different molecular weights, which provided precise control of dot size and periodicity of the printed structures. Using a thermal annealing method, different phases can be separated that enable the self-assembly capability. Figure 16 shows a complex pattern consisted with lines and droplets printed by EHD printing. With EHD printing technology, high-resolution, high density, multi-molecule weights, and shape changed patterns can be directly fabricated, which can potentially enhance their applications for

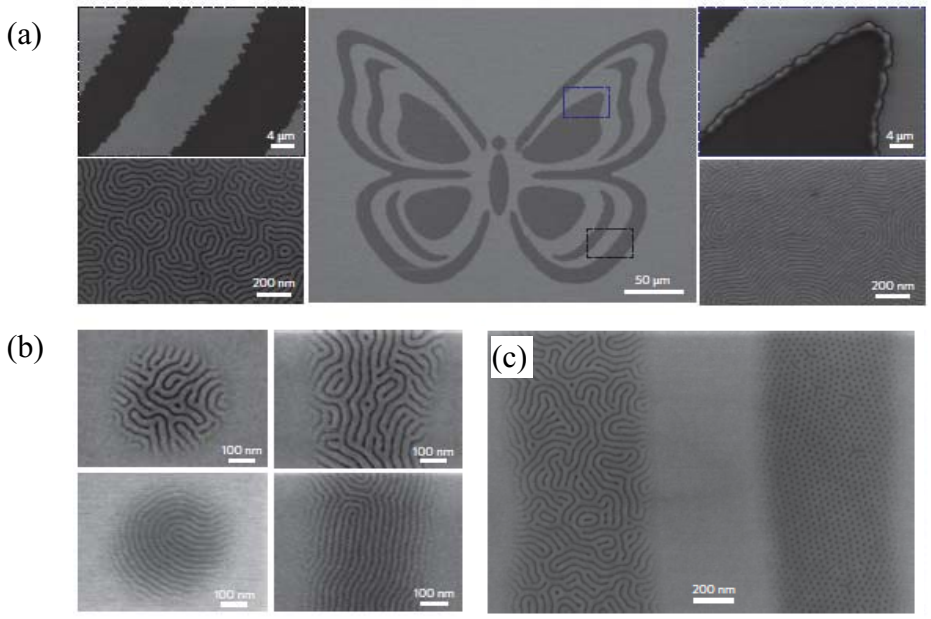

Figure 16: Electrohydrodynamic jet printing of BCP films. (a) SEM images of a complex pattern printed with two PS-b-PMMAs with different MWs. The left and right images present high-magnification views. (b) Individual dots (left) and lines (right) printed with 37-37 K (top) and 25-26 K (bottom) PS-b-PMMA (0.1% ink and a nozzle with 500 nm internal diameter). (c) SEM image showing self-assembled nanoscale structures with two different morphologies (lamellae forming 37-37 K, left; cylinder forming 46-21 K, right) printed as lines. Reproduced with permission [80]. Copyright 2013, Nature Publishing Group.

the fabrication of nano-devices. Currently, EHD printing for self-assembly applications is still at the very early stage and future investigations will be needed to further explore the potential applications of the EHD printed self-assembled structures.

The other direction of the self-assembly is to control the arrangement of the particles or wires in the printed features [95, 195]. With colloidal suspensions, the printed particles with different numbers self-assembled into a single particle during the evaporation of the liquid by the capillary force [195]. Lee et al. demonstrated that the orientation of the AgNWs in the printed line can also be controlled by EHD printing [94]. The length of the nanowires was about 20µm with a diameter of about 40nm. The nanowires was suspended in a water/ethanol solution and mixed with PEO solution to form a final solution with a AgNWs density from 1mg/ml to 25mg/ml. The printed nanowires was successfully aligned at the direction that was parallel to the printing direction due to the hydrodynamic force.

7. Conclusion

EHD printing is an emerging printing technology that is capable of producing high-resolution features for a wide range of functional materials onto various substrates, including unconventional flexible, stretchable, and uneven substrates. Taking the advantage of electrohydrodynamically induced flows, EHD printing offers unbeatable resolution capability and produces features at length scales that cannot be directly achieved with conventional inkjet printer systems, which present opportunities for further research with promising potential of applications in various fields. Many additive manufacturing processes rely on some form of printing or deposition technologies to build 3D objects layer-by-layer. The high-resolution counterparts of these printing/deposition technologies can be readily found in EHD printing as the EHD DoD printing and EHD direct jet writing, which represent new opportunities of EHD printing towards the application of high-resolution additive manufacturing. For this area, the continuous development of the printing processes, new printing systems, and advanced process control that can reliably deliver materials with high efficiency in three dimensions is critical for the advancement of the field and make EHD printing commercially competitive for future additive manufacturing industry. Biomanufacturing and healthcare represent another opportunity for EHD printing. EHD printing provides capabilities for high-resolution patterning of biomaterials, biomolecules, and even living cells safely onto a substrate or into 3D structures, which are critical tasks for advanced applications in tissue engineering and biotechnology. Printed electronics is one of the top applications for EHD printing, which has unique capabilities to deliver a wide range of functional materials that may not be compatible with the semiconductor manufacturing processes onto unconventional substrates, such as flexible/stretchable substrates and uneven curved surfaces. The demanding requirements from the modern electronics industry on reduction of critical feature sizes and large-scale integration of functions to achieve better performance make EHD printing a favorable approach for future printed electronics. More investigations on the functional inks and printing processes are under the way for many novel applications, including the applications in the optical systems and material self-assembly.

To further expand the scope and depth of EHD printing for the existing and new applications, research efforts will be needed to develop new printing systems and novel printing processes, and to achieve in-depth understanding of the process-material interaction. High throughput printing systems with advanced algorithms for process control will accelerate the transformation of EHD

printing technology from the research labs to commercially competitive manufacturing practice. The development of novel inks and the associated printing processes will foster new applications of the EHD printing technology to the broader research community. The ink design and process innovation demand a detailed understanding of the fundamental physics and mechanism of the printing process. Fully modeling the relationship among the material properties of the inks, the printing conditions, and the resulting printing behaviors (e.g. jetting modes, jet or droplet formation, etc.) will pave the way to fully utilize the EHD printing processes with advanced capabilities, such as designing inks with excellent printability, further improving the printing resolution and printing speed, developing printing systems with the best performance, etc.

Acknowledgments

This work was supported in part by the National Science Foundation under Grant Award CMMI-1333775 and CMMI-1728370.

Reference

[1] Madou, M. J., 2002, Fundamentals of microfabrication: the science of miniaturization, CRC press.

[2] Stepanova, M., and Dew, S., 2011, Nanofabrication: techniques and principles, Springer Science & Business Media.

[3] Robinson, G., and Jackson, M., 2005, "A review of micro and nanomachining from a materials perspective," Journal of materials processing technology, 167(2-3), pp. 316-337.

[4] Dornfeld, D., Min, S., and Takeuchi, Y., 2006, "Recent advances in mechanical micromachining," CIRP Annals-Manufacturing Technology, 55(2), pp. 745-768.

[5] Cheng, J., Liu, C.-s., Shang, S., Liu, D., Perrie, W., Dearden, G., and Watkins, K., 2013, "A review of ultrafast laser materials micromachining," Optics & Laser Technology, 46, pp. 88-102.

[6] Hutchings, I. M., and Martin, G. D., 2012, Inkjet technology for digital fabrication, John Wiley & Sons.

[7] Hoath, S. D., 2016, Fundamentals of inkjet printing: the science of inkjet and droplets, John Wiley & Sons.

[8] Sirringhaus, H., Kawase, T., Friend, R., Shimoda, T., Inbasekaran, M., Wu, W., and Woo, E., 2000, "High-resolution inkjet printing of all-polymer transistor circuits," Science, 290(5499), pp. 2123-2126.

[9] De Gans, B. J., Duineveld, P. C., and Schubert, U. S., 2004, "Inkjet printing of polymers: state of the art and future developments," Advanced materials, 16(3), pp. 203-213.

[10] Singh, M., Haverinen, H. M., Dhagat, P., and Jabbour, G. E., 2010, "Inkjet printing—process and its applications," Advanced materials, 22(6), pp. 673-685.

[11] Basaran, O. A., Gao, H., and Bhat, P. P., 2013, "Nonstandard inkjets," Annual Review of Fluid Mechanics, 45, pp. 85-113.

[12] Percin, G., and Khuri-Yakub, B. T., 2002, "Piezoelectrically actuated flextensional micromachined ultrasound droplet ejectors," IEEE transactions on ultrasonics, ferroelectrics, and frequency control, 49(6), pp. 756-766.

[13] Hyun, W. J., Secor, E. B., Hersam, M. C., Frisbie, C. D., and Francis, L. F., 2015, "High‐resolution patterning of graphene by screen printing with a silicon stencil for highly flexible printed electronics," Advanced Materials, 27(1), pp. 109-115.

[14] Dungchai, W., Chailapakul, O., and Henry, C. S., 2011, "A low-cost, simple, and rapid fabrication method for paper-based microfluidics using wax screen-printing," Analyst, 136(1), pp. 77-82.

[15] Hyun, W. J., Lim, S., Ahn, B. Y., Lewis, J. A., Frisbie, C. D., and Francis, L. F., 2015, "Screen printing of highly loaded silver inks on plastic substrates using silicon stencils," ACS applied materials & interfaces, 7(23), pp. 12619-12624.

[16] Khan, S., Lorenzelli, L., and Dahiya, R., 2014, "Technologies for printing sensors and electronics over large flexible substrates: a review," IEEE Sensors Journal, 15(6), pp. 3164-3185.

[17] Park, J.-U., Hardy, M., Kang, S. J., Barton, K., Adair, K., kishore Mukhopadhyay, D., Lee, C. Y., Strano, M. S., Alleyne, A. G., and Georgiadis, J. G., 2007, "High-resolution electrohydrodynamic jet printing," Nature materials, 6(10), pp. 782-789.

[18] Onses, M. S., Sutanto, E., Ferreira, P. M., Alleyne, A. G., and Rogers, J. A., 2015, "Mechanisms, capabilities, and applications of high‐resolution electrohydrodynamic jet printing," Small, 11(34), pp. 4237-4266.

[19] Zeleny, J., 1917, "Instability of electrified liquid surfaces," Physical review, 10(1), p. 1.

[20] Cloupeau, M., and Prunet-Foch, B., 1994, "Electrohydrodynamic spraying functioning modes: a critical review," Journal of Aerosol Science, 25(6), pp. 1021-1036.

[21] Fenn, J. B., Mann, M., Meng, C. K., Wong, S. F., and Whitehouse, C. M., 1990, "Electrospray ionization–principles and practice," Mass Spectrometry Reviews, 9(1), pp. 37-70.

[22] Jaworek, A., and Krupa, A., 1999, "Jet and drops formation in electrohydrodynamic spraying of liquids. A systematic approach," Experiments in fluids, 27(1), pp. 43-52.

[23] Sill, T. J., and von Recum, H. A., 2008, "Electrospinning: applications in drug delivery and tissue engineering," Biomaterials, 29(13), pp. 1989-2006.

[24] Gries, K., Vieker, H., Gölzhäuser, A., Agarwal, S., and Greiner, A., 2012, "Preparation of Continuous Gold Nanowires by Electrospinning of High‐Concentration Aqueous Dispersions of Gold Nanoparticles," Small, 8(9), pp. 1436-1441.

[25] Dalton, P. D., Joergensen, N. T., Groll, J., and Moeller, M., 2008, "Patterned melt electrospun substrates for tissue engineering," Biomedical Materials, 3(3), p. 034109.

[26] Sun, D., Chang, C., Li, S., and Lin, L., 2006, "Near-field electrospinning," Nano letters, 6(4), pp. 839-842.

[27] Jaworek, A., and Krupa, A., 1999, "Classification of the modes of EHD spraying," Journal of Aerosol Science, 30(7), pp. 873-893.

[28] Jaworek, A., and Krupa, A., "Main modes of electrohydrodynamic spraying of liquids," Proc. Third International Conference on multiphase Flow, pp. 8-12.

[29] Cloupeau, M., and Prunet-Foch, B., 1990, "Electrostatic spraying of liquids: main functioning modes," Journal of electrostatics, 25(2), pp. 165-184.

[30] Noymer, P. D., and Garel, M., 2000, "Stability and atomization characteristics of electrohydrodynamic jets in the cone-jet and multi-jet modes," Journal of aerosol science, 31(10), pp. 1165-1172.

[31] Lee, A., Jin, H., Dang, H.-W., Choi, K.-H., and Ahn, K. H., 2013, "Optimization of experimental parameters to determine the jetting regimes in electrohydrodynamic printing," Langmuir, 29(44), pp. 13630-13639.

[32] Hayati, I., Bailey, A., and Tadros, T. F., 1987, "Investigations into the mechanism of electrohydrodynamic spraying of liquids: II. Mechanism of stable jet formation and electrical forces acting on a liquid cone," Journal of colloid and interface science, 117(1), pp. 222-230.

[33] Hayati, I., Bailey, A., and Tadros, T. F., 1987, "Investigations into the mechanisms of electrohydrodynamic spraying of liquids: I. Effect of electric field and the environment on pendant drops and factors affecting the formation of stable jets and atomization," Journal of Colloid and Interface Science, 117(1), pp. 205-221.

[34] Scheideler, W. J., and Chen, C.-H., 2014, "The minimum flow rate scaling of Taylor cone-jets issued from a nozzle," Applied Physics Letters, 104(2), p. 024103.

[35] Jayasinghe, S., and Edirisinghe, M., 2004, "Electric-field driven jetting from dielectric liquids," Applied physics letters, 85(18), pp. 4243-4245.

[36] Marginean, I., Nemes, P., Parvin, L., and Vertes, A., 2006, "How much charge is there on a pulsating Taylor cone?," Applied physics letters, 89(6), p. 064104.

[37] Zhang, X., and Basaran, O. A., 1996, "Dynamics of drop formation from a capillary in the presence of an electric field," Journal of Fluid Mechanics, 326, pp. 239-263.

[38] Lee, M. W., Kim, N. Y., and Yoon, S. S., 2013, "On pinchoff behavior of electrified droplets," Journal of Aerosol Science, 57, pp. 114-124.

[39] Hartman, R., Brunner, D., Camelot, D., Marijnissen, J., and Scarlett, B., 2000, "Jet break-up in electrohydrodynamic atomization in the cone-jet mode," Journal of Aerosol Science, 31(1), pp. 65-95.

[40] Hartman, R., Brunner, D., Camelot, D., Marijnissen, J., and Scarlett, B., 1999, "Electrohydrodynamic atomization in the cone–jet mode physical modeling of the liquid cone and jet," Journal of Aerosol science, 30(7), pp. 823-849.

[41] Hartman, R., Marijnissen, J., and Scarlett, B., 1997, "Electro hydrodynamic atomization in the cone-jet mode. A physical model of the liquid cone and jet," Journal of Aerosol Science, 1001(28), pp. S527-S528.

[42] Lee, M., Kang, D., Kim, N., Kim, H., James, S., and Yoon, S., 2012, "A study of ejection modes for pulsed-DC electrohydrodynamic inkjet printing," Journal of Aerosol Science, 46, pp. 1-6.

[43] Stachewicz, U., Yurteri, C. U., Marijnissen, J. C., and Dijksman, J. F., 2009, "Stability regime of pulse frequency for single event electrospraying," Applied Physics Letters, 95(22), p. 224105.

[44] Bober, D. B., and Chen, C.-H., 2011, "Pulsating electrohydrodynamic cone-jets: from choked jet to oscillating cone," Journal of fluid mechanics, 689, pp. 552-563.

[45] Marginean, I., Parvin, L., Heffernan, L., and Vertes, A., 2004, "Flexing the electrified meniscus: The birth of a jet in electrosprays," Analytical chemistry, 76(14), pp. 4202-4207.

[46] Choi, H. K., Park, J.-U., Park, O. O., Ferreira, P. M., Georgiadis, J. G., and Rogers, J. A., 2008, "Scaling laws for jet pulsations associated with high-resolution electrohydrodynamic printing," Applied Physics Letters, 92(12), p. 123109.

[47] Song, C., Rogers, J. A., Kim, J.-M., and Ahn, H., 2015, "Patterned polydiacetylene-embedded polystyrene nanofibers based on electrohydrodynamic jet printing," Macromolecular Research, 23(1), pp. 118-123.

[48] Fernández de La Mora, J., 2007, "The fluid dynamics of Taylor cones," Annu. Rev. Fluid Mech., 39, pp. 217-243.

[49] Mestel, A., 1996, "Electrohydrodynamic stability of a highly viscous jet," Journal of Fluid Mechanics, 312, pp. 311-326.

[50] Kim, H. J., and Um, I. C., 2014, "Relationship between rheology and electro-spinning performance of regenerated silk fibroin prepared using different degumming methods," Korea-Australia Rheology Journal, 26(2), pp. 119-125.

[51] Lee, S.-H., Nguyen, X. H., and Ko, H. S., 2012, "Study on droplet formation with surface tension for electrohydrodynamic inkjet nozzle," Journal of mechanical science and technology, 26(5), pp. 1403-1408.

[52] Barrero, A., Ganan-Calvo, A., Davila, J., Palacios, A., and Gomez-Gonzalez, E., 1999, "The role of the electrical conductivity and viscosity on the motions inside Taylor cones," Journal of electrostatics, 47(1-2), pp. 13-26.

[53] Yu, M., Ahn, K. H., and Lee, S. J., 2016, "Design optimization of ink in electrohydrodynamic jet printing: Effect of viscoelasticity on the formation of Taylor cone jet," Materials & Design, 89, pp. 109-115.

[54] Bae, J., Lee, J., and Hyun Kim, S., 2017, "Effects of polymer properties on jetting performance of electrohydrodynamic printing," Journal of Applied Polymer Science, 134(35), p. 45044.

[55] Park, J., and Hwang, J., 2014, "Fabrication of a flexible Ag-grid transparent electrode using ac based electrohydrodynamic Jet printing," Journal of Physics D: Applied Physics, 47(40), p. 405102.

[56] Yu, J., Kim, S., and Hwang, J., 2007, "Effect of viscosity of silver nanoparticle suspension on conductive line patterned by electrohydrodynamic jet printing," Applied Physics A, 89(1), pp. 157-159.

[57] Prasetyo, F. D., Yudistira, H. T., Nguyen, V. D., and Byun, D., 2013, "Ag dot morphologies printed using electrohydrodynamic (EHD) jet printing based on a drop-on-demand (DOD) operation," Journal of Micromechanics and Microengineering, 23(9), p. 095028.

[58] Wei, C., Qin, H., Ramírez-Iglesias, N. A., Chiu, C.-P., Lee, Y.-s., and Dong, J., 2014, "High-resolution ac-pulse modulated electrohydrodynamic jet printing on highly insulating substrates," Journal of Micromechanics and Microengineering, 24(4), p. 045010.

[59] Lee, D.-Y., Shin, Y.-S., Park, S.-E., Yu, T.-U., and Hwang, J., 2007, "Electrohydrodynamic printing of silver nanoparticles by using a focused nanocolloid jet," Applied Physics Letters, 90(8), p. 081905.

[60] Rahman, K., Khan, A., Muhammad, N. M., Jo, J., and Choi, K.-H., 2012, "Fine-resolution patterning of copper nanoparticles through electrohydrodynamic jet printing," Journal of Micromechanics and Microengineering, 22(6), p. 065012.

[61] Jayasinghe, S., Edirisinghe, M., and Wang, D., 2004, "Controlled deposition of nanoparticle clusters by electrohydrodynamic atomization," Nanotechnology, 15(11), p. 1519.

[62] Kang, D., Lee, M., Kim, H., James, S., and Yoon, S., 2011, "Electrohydrodynamic pulsed-inkjet characteristics of various inks containing aluminum particles," Journal of Aerosol Science, 42(10), pp. 621-630.

[63] Wang, D., Jayasinghe, S., and Edirisinghe, M., 2005, "High resolution print-patterning of a nano-suspension," Journal of Nanoparticle Research, 7(2-3), pp. 301-306.

[64] Wang, D., Edirisinghe, M., and Jayasinghe, S., 2006, "Solid Freeform Fabrication of Thin‐Walled Ceramic Structures Using an Electrohydrodynamic Jet," Journal of the American Ceramic Society, 89(5), pp. 1727-1729.

[65] Sabaeian, M., and Khaledi-Nasab, A., 2012, "Size-dependent intersubband optical properties of dome-shaped InAs/GaAs quantum dots with wetting layer," Applied optics, 51(18), pp. 4176-4185.

[66] Khaledi-Nasab, A., Sabaeian, M., Sahrai, M., and Fallahi, V., 2014, "Kerr nonlinearity due to intersubband transitions in a three-level InAs/GaAs quantum dot: the impact of a wetting layer on dispersion curves," Journal of Optics, 16(5), p. 055004.

[67] Kim, J. Y., Voznyy, O., Zhitomirsky, D., and Sargent, E. H., 2013, "25th Anniversary Article: Colloidal Quantum Dot Materials and Devices: A Quarter‐Century of Advances," Advanced Materials, 25(36), pp. 4986-5010.

[68] Kim, B. H., Onses, M. S., Lim, J. B., Nam, S., Oh, N., Kim, H., Yu, K. J., Lee, J. W., Kim, J.-H., and Kang, S.-K., 2015, "High-resolution patterns of quantum dots formed by electrohydrodynamic jet printing for light-emitting diodes," Nano letters, 15(2), pp. 969-973.

[69] Gupta, A., Seifalian, A. M., Ahmad, Z., Edirisinghe, M. J., and Winslet, M. C., 2007, "Novel electrohydrodynamic printing of nanocomposite biopolymer scaffolds," Journal of bioactive and compatible polymers, 22(3), pp. 265-280.

[70] Poellmann, M. J., and Johnson, A. J. W., 2014, "Multimaterial polyacrylamide: Fabrication with electrohydrodynamic jet printing, applications, and modeling," Biofabrication, 6(3), p. 035018.

[71] Reneker, D. H., and Yarin, A. L., 2008, "Electrospinning jets and polymer nanofibers," Polymer, 49(10), pp. 2387-2425.

[72] Nothnagle, C., Baptist, J. R., Sanford, J., Lee, W. H., Popa, D. O., and Wijesundara, M. B., "EHD printing of PEDOT: PSS inks for fabricating pressure and strain sensor arrays on flexible substrates," Proc. Next-Generation Robotics II; and Machine Intelligence and Bio-inspired Computation: Theory and Applications IX, International Society for Optics and Photonics, p. 949403.

[73] Park, S. H., Kim, J., Park, C. E., Lee, J., Lee, H. S., Lim, S., and Kim, S. H., 2016, "Optimization of electrohydrodynamic-printed organic electrodes for bottom-contact organic thin film transistors," Organic Electronics, 38, pp. 48-54.

[74] Han, Y., Wei, C., and Dong, J., 2015, "Droplet formation and settlement of phase-change ink in high resolution electrohydrodynamic (EHD) 3D printing," Journal of Manufacturing Processes, 20, pp. 485-491.

[75] Theron, S., Zussman, E., and Yarin, A., 2004, "Experimental investigation of the governing parameters in the electrospinning of polymer solutions," Polymer, 45(6), pp. 2017-2030.

[76] Lee, M.-W., Lee, M.-Y., Choi, J.-C., Park, J.-S., and Song, C.-K., 2010, "Fine patterning of glycerol-doped PEDOT: PSS on hydrophobic PVP dielectric with ink jet for source and drain electrode of OTFTs," Organic Electronics, 11(5), pp. 854-859.

[77] Bihar, E., Roberts, T., Saadaoui, M., Herv J.-S., and Song, C.-K., 2010, "Fine patterning of glycerol‐Printed PEDOT: PSS Electrodes on Paper for Electrocardiography," Advanced healthcare materials, 6(6), p. 1601167.

[78] Vuorinen, T., Niittynen, J., Kankkunen, T., Kraft, T. M., and Mäntysalo, M., 2016, "Inkjet-printed graphene/PEDOT: PSS temperature sensors on a skin-conformable polyurethane substrate," Scientific reports, 6, p. 35289.

[79] Jang, S., Kim, Y., and Oh, J. H., 2016, "Influence of processing conditions and material properties on electrohydrodynamic direct patterning of a polymer solution," Journal of Electronic Materials, 45(4), pp. 2291-2298.

[80] Onses, M. S., Song, C., Williamson, L., Sutanto, E., Ferreira, P. M., Alleyne, A. G., Nealey, P. F., Ahn, H., and Rogers, J. A., 2013, "Hierarchical patterns of three-dimensional block-copolymer films formed by electrohydrodynamic jet printing and self-assembly," Nature nanotechnology, 8(9), p. 667.

[81] Park, J.-U., Lee, J. H., Paik, U., Lu, Y., and Rogers, J. A., 2008, "Nanoscale patterns of oligonucleotides formed by electrohydrodynamic jet printing with applications in biosensing and nanomaterials assembly," Nano letters, 8(12), pp. 4210-4216.

[82] Shigeta, K., He, Y., Sutanto, E., Kang, S., Le, A.-P., Nuzzo, R. G., Alleyne, A. G., Ferreira, P. M., Lu, Y., and Rogers, J. A., 2012, "Functional protein microarrays by electrohydrodynamic jet printing," Analytical chemistry, 84(22), pp. 10012-10018.

[83] Lee, J.-G., Cho, H.-J., Huh, N., Ko, C., Lee, W.-C., Jang, Y.-H., Lee, B. S., Kang, I. S., and Choi, J.-W., 2006, "Electrohydrodynamic (EHD) dispensing of nanoliter DNA droplets for microarrays," Biosensors and Bioelectronics, 21(12), pp. 2240-2247.

[84] Wei, C., and Dong, J., 2013, "Direct fabrication of high-resolution three-dimensional polymeric scaffolds using electrohydrodynamic hot jet plotting," Journal of Micromechanics and Microengineering, 23(2), p. 025017.

[85] Han, Y., and Dong, J., 2017, "High-resolution direct printing of molten-metal using electrohydrodynamic jet plotting," Manufacturing Letters, 12, pp. 6-9.

[86] Boley, J. W., White, E. L., Chiu, G. T. C., and Kramer, R. K., 2014, "Direct writing of gallium‐indium alloy for stretchable electronics," Advanced Functional Materials, 24(23), pp. 3501-3507.

[87] Lee, T.-M., Kang, T. G., Yang, J.-S., Jo, J.-D., Kim, K.-Y., Choi, B.-O., and Kim, D.-S., "3D metal microstructure fabrication using a molten metal DoD inkjet system," Proc. Solid-State Sensors, Actuators and Microsystems Conference, 2007. TRANSDUCERS 2007. International, IEEE, pp. 1637-1640.

[88] Wang, Q., Yu, Y., Yang, J., and Liu, J., 2015, "Fast fabrication of flexible functional circuits based on liquid metal dual‐trans printing," Advanced Materials, 27(44), pp. 7109-7116.

[89] Lee, T.-M., Kang, T. G., Yang, J. S., Jo, J., Kim, K.-Y., Choi, B.-O., and Kim, D.-S., 2008, "Gap adjustable molten metal DoD inkjet system with cone-shaped piston head," Journal of manufacturing science and engineering, 130(3), p. 031113.

[90] Murr, L. E., Gaytan, S. M., Ramirez, D. A., Martinez, E., Hernandez, J., Amato, K. N., Shindo, P. W., Medina, F. R., and Wicker, R. B., 2012, "Metal fabrication by additive manufacturing using laser and electron beam melting technologies," Journal of Materials Science & Technology, 28(1), pp. 1-14.

[91] Agarwala, M., Bourell, D., Beaman, J., Marcus, H., and Barlow, J., 1995, "Direct selective laser sintering of metals," Rapid Prototyping Journal, 1(1), pp. 26-36.

[92] Langley, D., Giusti, G., Mayousse, C., Celle, C., Bellet, D., and Simonato, J.-P., 2013, "Flexible transparent conductive materials based on silver nanowire networks: a review," Nanotechnology, 24(45), p. 452001.

[93] Yao, S., and Zhu, Y., 2015, "Nanomaterial‐enabled stretchable conductors: strategies, materials and devices," Advanced materials, 27(9), pp. 1480-1511.

[94] Lee, H., Seong, B., Kim, J., Jang, Y., and Byun, D., 2014, "Direct alignment and patterning of silver nanowires by electrohydrodynamic jet printing," Small, 10(19), pp. 3918-3922.

[95] Cui, Z., Han, Y., Huang, Q., Dong, J., and Zhu, Y., 2018, "Electrohydrodynamic printing of silver nanowires for flexible and stretchable electronics," Nanoscale, 10(15), pp. 6806-6811.

[96] An, B. W., Kim, K., Kim, M., Kim, S. Y., Hur, S. H., and Park, J. U., 2015, "Direct printing of reduced graphene oxide on planar or highly curved surfaces with high resolutions using electrohydrodynamics," Small, 11(19), pp. 2263-2268.

[97] Lee, S., An, K., Son, S., and Choi, J., 2013, "Satellite/spray suppression in electrohydrodynamic printing with a gated head," Applied Physics Letters, 103(13), p. 133506.

[98] Xu, L., and Sun, D., 2013, "Electrohydrodynamic printing under applied pole-type nozzle configuration," Applied Physics Letters, 102(2), p. 024101.

[99] Choi, J., Kim, Y.-J., Lee, S., Son, S. U., Ko, H. S., Nguyen, V. D., and Byun, D., 2008, "Drop-on-demand printing of conductive ink by electrostatic field induced inkjet head," Applied Physics Letters, 93(19), p. 193508.

[100] Kim, H., Song, J., Chung, J., and Hong, D., 2010, "Onset condition of pulsating cone-jet mode of electrohydrodynamic jetting for plane, hole, and pin type electrodes," Journal of Applied Physics, 108(10), p. 102804.

[101] Tse, L., and Barton, K., 2015, "Airflow assisted printhead for high-resolution electrohydrodynamic jet printing onto non-conductive and tilted surfaces," Applied Physics Letters, 107(5), p. 054103.

[102] Tse, L., and Barton, K., 2014, "A field shaping printhead for high-resolution electrohydrodynamic jet printing onto non-conductive and uneven surfaces," Applied Physics Letters, 104(14), p. 143510.

[103] Han, Y., and Dong, J., 2017, "Design, modeling and testing of integrated ring extractor for high resolution electrohydrodynamic (EHD) 3D printing," Journal of Micromechanics and Microengineering, 27(3), p. 035005.

[104] Han, Y., Wei, C., and Dong, J., 2014, "Super-resolution electrohydrodynamic (EHD) 3D printing of micro-structures using phase-change inks," Manufacturing Letters, 2(4), pp. 96-99.

[105] Kim, S.-Y., Kim, Y., Park, J., and Hwang, J., 2010, "Design and evaluation of single nozzle with a non-conductive tip for reducing applied voltage and pattern width in electrohydrodynamic jet printing (EHDP)," Journal of Micromechanics and Microengineering, 20(5), p. 055009.

[106] Barton, K., Mishra, S., Shorter, K. A., Alleyne, A., Ferreira, P., and Rogers, J., 2010, "A desktop electrohydrodynamic jet printing system," Mechatronics, 20(5), pp. 611-616.

[107] Pan, Y., Huang, Y., Guo, L., Ding, Y., and Yin, Z., 2015, "Addressable multi-nozzle electrohydrodynamic jet printing with high consistency by multi-level voltage method," AIP Advances, 5(4), p. 047108.

[108] Khan, A., Rahman, K., Kim, D. S., and Choi, K. H., 2012, "Direct printing of copper conductive micro-tracks by multi-nozzle electrohydrodynamic inkjet printing process," Journal of materials processing technology, 212(3), pp. 700-706.

[109] Khan, A., Rahman, K., Hyun, M.-T., Kim, D.-S., and Choi, K.-H., 2011, "Multi-nozzle electrohydrodynamic inkjet printing of silver colloidal solution for the fabrication of electrically functional microstructures," Applied Physics A, 104(4), p. 1113.

[110] Lee, J.-S., Kim, S.-Y., Kim, Y.-J., Park, J., Kim, Y., Hwang, J., and Kim, Y.-J., 2008, "Design and evaluation of a silicon based multi-nozzle for addressable jetting using a controlled flow rate in electrohydrodynamic jet printing," Applied Physics Letters, 93(24), p. 243114.

[111] Sutanto, E., Shigeta, K., Kim, Y., Graf, P., Hoelzle, D., Barton, K., Alleyne, A., Ferreira, P., and Rogers, J., 2012, "A multimaterial electrohydrodynamic jet (E-jet) printing system," Journal of Micromechanics and Microengineering, 22(4), p. 045008.

[112] Galliker, P., Schneider, J., Eghlidi, H., Kress, S., Sandoghdar, V., and Poulikakos, D., 2012, "Direct printing of nanostructures by electrostatic autofocussing of ink nanodroplets," Nature communications, 3, p. 890.

[113] Xing, B., Zuo, C. C., Huang, F. L., Lu, Y. B., and Hu, G. S., "Effect of Electrode Distance on Jetting Behavior of Non-Particle Nano Ag Conductive Ink in Electrohydrodynamic Micro Jet Printing," Proc. Materials Science Forum, Trans Tech Publ, pp. 118-121.

[114] Chen, C.-H., Saville, D., and Aksay, I., 2006, "Electrohydrodynamic “drop-and-place” particle deployment," Applied physics letters, 88(15), p. 154104.

[115] Wei, C., and Dong, J., 2014, "Development and modeling of melt electrohydrodynamic-jet printing of phase-change inks for high-resolution additive manufacturing," Journal of Manufacturing Science and Engineering, 136(6), p. 061010.

[116] Mishra, S., Barton, K. L., Alleyne, A. G., Ferreira, P. M., and Rogers, J. A., 2010, "High-speed and drop-on-demand printing with a pulsed electrohydrodynamic jet," Journal of Micromechanics and Microengineering, 20(9), p. 095026.

[117] Park, J., Kim, B., Kim, S.-Y., and Hwang, J., 2014, "Prediction of drop-on-demand (DOD) pattern size in pulse voltage-applied electrohydrodynamic (EHD) jet printing of Ag colloid ink," Applied Physics A, 117(4), pp. 2225-2234.

[118] Kim, J., Oh, H., and Kim, S. S., 2008, "Electrohydrodynamic drop-on-demand patterning in pulsed cone-jet mode at various frequencies," Journal of Aerosol Science, 39(9), pp. 819-825.

[119] Lee, S., Song, J., Kim, H., and Chung, J., 2012, "Time resolved imaging of electrohydrodynamic jetting on demand induced by square pulse voltage," Journal of Aerosol Science, 52, pp. 89-97.

[120] Rahman, K., Khan, A., Nam, N. M., Choi, K. H., and Kim, D.-S., 2011, "Study of drop-on-demand printing through multi-step pulse voltage," International Journal of Precision Engineering and Manufacturing, 12(4), pp. 663-669.

[121] Lee, M. W., An, S., Kim, N. Y., Seo, J. H., Huh, J.-Y., Kim, H. Y., and Yoon, S. S., 2013, "Effects of pulsing frequency on characteristics of electrohydrodynamic inkjet using micro-Al and nano-Ag particles," Experimental Thermal and Fluid Science, 46, pp. 103-110.

[122] Xu, L., Wang, X., Lei, T., Sun, D., and Lin, L., 2011, "Electrohydrodynamic deposition of polymeric droplets under low-frequency pulsation," Langmuir, 27(10), pp. 6541-6548.

[123] Wei, C., Qin, H., Chiu, C.-P., Lee, Y.-S., and Dong, J., 2015, "Drop-on-demand E-jet printing of continuous interconnects with AC-pulse modulation on highly insulating substrates," Journal of Manufacturing Systems, 37, pp. 505-510.

[124] Kim, Y.-J., Kim, S., Hwang, J., and Kim, Y.-J., 2013, "Drop-on-demand hybrid printing using a piezoelectric MEMS printhead at various waveforms, high voltages and jetting frequencies," Journal of Micromechanics and Microengineering, 23(6), p. 065011.

[125] Park, J., Park, J.-W., Nasrabadi, A. M., and Hwang, J., 2016, "Methodology to set up nozzle-to-substrate gap for high resolution electrohydrodynamic jet printing," Applied Physics Letters, 109(13), p. 134104.

[126] Jang, Y., Hartarto Tambunan, I., Tak, H., Dat Nguyen, V., Kang, T., and Byun, D., 2013, "Non-contact printing of high aspect ratio Ag electrodes for polycrystalline silicone solar cell with electrohydrodynamic jet printing," Applied Physics Letters, 102(12), p. 123901.

[127] Wu, Y., Wang, Z., Ying Hsi Fuh, J., San Wong, Y., Wang, W., and San Thian, E., 2017, "Direct E‐jet printing of three‐dimensional fibrous scaffold for tendon tissue engineering," Journal of Biomedical Materials Research Part B: Applied Biomaterials, 105(3), pp. 616-627.

[128] Jeong, S., Lee, S. H., Jo, Y., Lee, S. S., Seo, Y.-H., Ahn, B. W., Kim, G., Jang, G.-E., Park, J.-U., and Ryu, B.-H., 2013, "Air-stable, surface-oxide free Cu nanoparticles for highly conductive Cu ink and their application to printed graphene transistors," Journal of Materials Chemistry C, 1(15), pp. 2704-2710.

[129] Jeong, Y. J., Lee, X., Bae, J., Jang, J., Joo, S. W., Lim, S., Kim, S. H., and Park, C. E., 2016, "Direct patterning of conductive carbon nanotube/polystyrene sulfonate composites via electrohydrodynamic jet printing for use in organic field-effect transistors," Journal of Materials Chemistry C, 4(22), pp. 4912-4919.

[130] Seong, B., Yoo, H., Nguyen, V. D., Jang, Y., Ryu, C., and Byun, D., 2014, "Metal-mesh based transparent electrode on a 3-D curved surface by electrohydrodynamic jet printing," Journal of Micromechanics and Microengineering, 24(9), p. 097002.

[131] Wei, C., and Dong, J., 2014, "Hybrid hierarchical fabrication of three-dimensional scaffolds," Journal of Manufacturing Processes, 16(2), pp. 257-263.

[132] Zhang, B., Seong, B., Nguyen, V., and Byun, D., 2016, "3D printing of high-resolution PLA-based structures by hybrid electrohydrodynamic and fused deposition modeling techniques," Journal of Micromechanics and Microengineering, 26(2), p. 025015.

[133] Chen, C.-H., Saville, D., and Aksay, I., 2006, "Scaling laws for pulsed electrohydrodynamic drop formation," Applied Physics Letters, 89(12), p. 124103.

[134] Du, W., and Chaudhuri, S., 2017, "A multiphysics model for charged liquid droplet breakup in electric fields," International Journal of Multiphase Flow, 90, pp. 46-56.

[135] Kim, Y.-J., Choi, J., Son, S. U., Lee, S., Nguyen, X. H., Nguyen, V. D., Byun, D., and Ko, H. S., 2010, "Comparative Study on Ejection Phenomena of Droplets from Electro-Hydrodynamic Jet by Hydrophobic and Hydrophilic Coatings of Nozzles," Japanese Journal of Applied Physics, 49(6R), p. 060217.

[136] Yudistira, H. T., Nguyen, V. D., Dutta, P., and Byun, D., 2010, "Flight behavior of charged droplets in electrohydrodynamic inkjet printing," Applied Physics Letters, 96(2), p. 023503.

[137] Collins, R. T., Harris, M. T., and Basaran, O. A., 2007, "Breakup of electrified jets," Journal of Fluid Mechanics, 588, pp. 75-129.

[138] Mestel, A., 1994, "The electrohydrodynamic cone-jet at high Reynolds number," Journal of aerosol science, 25(6), pp. 1037-1047.

[139] Ganan-Calvo, A. M., 1997, "On the theory of electrohydrodynamically driven capillary jets," Journal of Fluid Mechanics, 335, pp. 165-188.

[140] Wei, W., Gu, Z., Wang, S., Zhang, Y., Lei, K., and Kase, K., 2012, "Numerical simulation of the cone–jet formation and current generation in electrostatic spray—modeling as regards space charged droplet effect," Journal of Micromechanics and Microengineering, 23(1), p. 015004.

[141] Collins, R. T., Sambath, K., Harris, M. T., and Basaran, O. A., 2013, "Universal scaling laws for the disintegration of electrified drops," Proceedings of the National Academy of Sciences, p. 201213708.

[142] Yan, F., Farouk, B., and Ko, F., 2003, "Numerical modeling of an electrostatically driven liquid meniscus in the cone–jet mode," Journal of Aerosol Science, 34(1), pp. 99-116.

[143] Pannier, C. P., Diagne, M., Spiegel, I. A., Hoelzle, D. J., and Barton, K., 2017, "A Dynamical Model of Drop Spreading in Electrohydrodynamic Jet Printing," Journal of Manufacturing Science and Engineering, 139(11), p. 111008.

[144] Rahmat, A., Koç, B., and Yildiz, M., 2017, "A systematic study on numerical simulation of electrified jet printing," Additive Manufacturing, 18, pp. 15-21.

[145] Tran, S. B. Q., Byun, D., Nguyen, V. D., and Kang, T. S., 2009, "Liquid meniscus oscillation and drop ejection by ac voltage, pulsed dc voltage, and superimposing dc to ac voltages," Physical Review E, 80(2), p. 026318.

[146] Nguyen, V. D., and Byun, D., 2009, "Mechanism of electrohydrodynamic printing based on ac voltage without a nozzle electrode," Applied Physics Letters, 94(17), p. 173509.

[147] Ashley, S., 1991, "Rapid prototyping systems," Mechanical Engineering, 113(4), p. 34.

[148] Mueller, B., 2012, "Additive manufacturing technologies–Rapid prototyping to direct digital manufacturing," Assembly Automation, 32(2).

[149] Kruth, J.-P., Leu, M.-C., and Nakagawa, T., 1998, "Progress in additive manufacturing and rapid prototyping," Cirp Annals, 47(2), pp. 525-540.

[150] Melchels, F. P., Domingos, M. A., Klein, T. J., Malda, J., Bartolo, P. J., and Hutmacher, D. W., 2012, "Additive manufacturing of tissues and organs," Progress in Polymer Science, 37(8), pp. 1079-1104.

[151] Kruth, J.-P., 1991, "Material incress manufacturing by rapid prototyping techniques," CIRP Annals-Manufacturing Technology, 40(2), pp. 603-614.

[152] An, B. W., Kim, K., Lee, H., Kim, S. Y., Shim, Y., Lee, D. Y., Song, J. Y., and Park, J. U., 2015, "High‐resolution printing of 3D structures using an electrohydrodynamic inkjet with multiple functional inks," Advanced Materials, 27(29), pp. 4322-4328.

[153] Brown, T. D., Dalton, P. D., and Hutmacher, D. W., 2011, "Direct writing by way of melt electrospinning," Advanced Materials, 23(47), pp. 5651-5657.

[154] Zhao, X., He, J., Xu, F., Liu, Y., and Li, D., 2016, "Electrohydrodynamic printing: A potential tool for high-resolution hydrogel/cell patterning," Virtual and Physical Prototyping, 11(1), pp. 57-63.

[155] Jayasinghe, S. N., Qureshi, A. N., and Eagles, P. A., 2006, "Electrohydrodynamic jet processing: an advanced electric‐field‐driven jetting phenomenon for processing living cells," Small, 2(2), pp. 216-219.

[156] Eagles, P. A., Qureshi, A. N., and Jayasinghe, S. N., 2006, "Electrohydrodynamic jetting of mouse neuronal cells," Biochemical Journal, 394(2), pp. 375-378.

[157] Faulkner-Jones, A., Greenhough, S., King, J. A., Gardner, J., Courtney, A., and Shu, W., 2013, "Development of a valve-based cell printer for the formation of human embryonic stem cell spheroid aggregates," Biofabrication, 5(1), p. 015013.

[158] Mehta, P., Haj-Ahmad, R., Rasekh, M., Arshad, M. S., Smith, A., van der Merwe, S. M., Li, X., Chang, M.-W., and Ahmad, Z., 2017, "Pharmaceutical and biomaterial engineering via electrohydrodynamic atomization technologies," Drug discovery today, 22(1), pp. 157-165.

[159] Kim, J.-H., Lee, D.-Y., Hwang, J., and Jung, H.-I., 2009, "Direct pattern formation of bacterial cells using micro-droplets generated by electrohydrodynamic forces," Microfluidics and nanofluidics, 7(6), p. 829.

[160] Gasperini, L., Maniglio, D., Motta, A., and Migliaresi, C., 2014, "An electrohydrodynamic bioprinter for alginate hydrogels containing living cells," Tissue Engineering Part C: Methods, 21(2), pp. 123-132.

[161] Ringeisen, B. R., Othon, C. M., Barron, J. A., Young, D., and Spargo, B. J., 2006, "Jet‐based methods to print living cells," Biotechnology Journal: Healthcare Nutrition Technology, 1(9), pp. 930-948.

[162] Xu, T., Jin, J., Gregory, C., Hickman, J. J., and Boland, T., 2005, "Inkjet printing of viable mammalian cells," Biomaterials, 26(1), pp. 93-99.

[163] Liu, Y., Jiang, C., Liu, Y., Li, D., and Hu, Q., "Electrohydrodynamic direct printing on hydrogel: a novel method to obtain fine fibers," Proc. Biosensing and Nanomedicine IX, International Society for Optics and Photonics, p. 993010.

[164] Poellmann, M. J., Barton, K. L., Mishra, S., and Johnson, A. J. W., 2011, "Patterned hydrogel substrates for cell culture with electrohydrodynamic jet printing," Macromolecular bioscience, 11(9), pp. 1164-1168.

[165] Gasperini, L., Maniglio, D., and Migliaresi, C., 2013, "Microencapsulation of cells in alginate through an electrohydrodynamic process," Journal of Bioactive and Compatible Polymers, 28(5), pp. 413-425.

[166] Liaudanskaya, V., Gasperini, L., Maniglio, D., Motta, A., and Migliaresi, C., 2015, "Assessing the impact of electrohydrodynamic jetting on encapsulated cell viability, proliferation, and ability to self-assemble in three-dimensional structures," Tissue Engineering Part C: Methods, 21(6), pp. 631-638.

[167] Xu, T., Petridou, S., Lee, E. H., Roth, E. A., Vyavahare, N. R., Hickman, J. J., and Boland, T., 2004, "Construction of high‐density bacterial colony arrays and patterns by the ink‐jet method," Biotechnology and bioengineering, 85(1), pp. 29-33.

[168] Ahmad, Z., Rasekh, M., and Edirisinghe, M., 2010, "Electrohydrodynamic direct writing of biomedical polymers and composites," Macromolecular Materials and Engineering, 295(4), pp. 315-319.

[169] Kim, H. S., Lee, D. Y., Park, J. H., Kim, J. H., Hwang, J. H., and Jung, H. I., 2007, "Optimization of electrohydrodynamic writing technique to print collagen," Experimental techniques, 31(4), pp. 15-19.

[170] Cheung, H.-Y., Lau, K.-T., Lu, T.-P., and Hui, D., 2007, "A critical review on polymer-based bio-engineered materials for scaffold development," Composites Part B: Engineering, 38(3), pp. 291-300.

[171] George, M. C., and Braun, P. V., 2009, "Multicompartmental materials by electrohydrodynamic cojetting," Angewandte Chemie International Edition, 48(46), pp. 8606-8609.

[172] Li, J. L., Cai, Y. L., Guo, Y. L., Fuh, J. Y. H., Sun, J., Hong, G. S., Lam, R. N., Wong, Y. S., Wang, W., and Tay, B. Y., 2014, "Fabrication of three‐dimensional porous scaffolds with controlled filament orientation and large pore size via an improved E‐jetting technique," Journal of Biomedical Materials Research Part B: Applied Biomaterials, 102(4), pp. 651-658.

[173] Wu, Y., Fuh, J., Wong, Y., and Sun, J., "Fabrication of 3D scaffolds via E-jet printing for tendon tissue repair," Proc. ASME 2015 international manufacturing science and engineering conference, American Society of Mechanical Engineers, pp. V002T003A005-V002T003A005.

[174] Wang, H., Vijayavenkataraman, S., Wu, Y., Shu, Z., Sun, J., and Fuh, J. Y. H., 2016, "Investigation of process parameters of electrohydro-dynamic jetting for 3D printed PCL

fibrous scaffolds with complex geometries," International Journal of Bioprinting, 2(1), pp. 63-71.

[175] Liu, T., Huang, R., Zhong, J., Yang, Y., Tan, Z., and Tan, W., 2017, "Control of cell proliferation in E-jet 3D-printed scaffolds for tissue engineering applications: the influence of the cell alignment angle," Journal of Materials Chemistry B, 5(20), pp. 3728-3738.

[176] Hwang, T. H., Kim, Y. J., Chung, H., and Ryu, W., 2016, "Motionless electrohydrodynamic (EHD) printing of biodegradable polymer micro patterns," Microelectronic Engineering, 161, pp. 43-51.

[177] Awais, M. N., Kim, H. C., Doh, Y. H., and Choi, K. H., 2013, "ZrO2 flexible printed resistive (memristive) switch through electrohydrodynamic printing process," Thin Solid Films, 536, pp. 308-312.

[178] Khan, S., Doh, Y. H., Khan, A., Rahman, A., Choi, K. H., and Kim, D. S., 2011, "Direct patterning and electrospray deposition through EHD for fabrication of printed thin film transistors," Current applied physics, 11(1), pp. S271-S279.

[179] Gao-Feng, Z., Yan-Bo, P., Xiang, W., Jian-Yi, Z., and Dao-Heng, S., 2014, "Electrohydrodynamic direct—writing of conductor—insulator-conductor multi-layer interconnection," Chinese Physics B, 23(6), p. 066102.

[180] Wang, X., Xu, L., Zheng, G., Cheng, W., and Sun, D., 2012, "Pulsed electrohydrodynamic printing of conductive silver patterns on demand," Science china technological sciences, 55(6), pp. 1603-1607.

[181] Wang, K., and Stark, J. P., 2010, "Direct fabrication of electrically functional microstructures by fully voltage-controlled electrohydrodynamic jet printing of silver nano-ink," Applied Physics A, 99(4), pp. 763-766.

[182] Kim, S.-Y., Kim, K., Hwang, Y., Park, J., Jang, J., Nam, Y., Kang, Y., Kim, M., Park, H., and Lee, Z., 2016, "High-resolution electrohydrodynamic inkjet printing of stretchable metal oxide semiconductor transistors with high performance," Nanoscale, 8(39), pp. 17113-17121.

[183] Qin, H., Cai, Y., Dong, J., and Lee, Y.-S., 2017, "Direct Printing of Capacitive Touch Sensors on Flexible Substrates by Additive E-Jet Printing With Silver Nanoinks," Journal of Manufacturing Science and Engineering, 139(3), p. 031011.

[184] Pikul, J. H., Graf, P., Mishra, S., Barton, K., Kim, Y.-K., Rogers, J. A., Alleyne, A., Ferreira, P. M., and King, W. P., 2011, "High precision electrohydrodynamic printing of polymer onto microcantilever sensors," University of Illinois.

[185] Lee, S., Kim, J., Choi, J., Park, H., Ha, J., Kim, Y., Rogers, J. A., and Paik, U., 2012, "Patterned oxide semiconductor by electrohydrodynamic jet printing for transparent thin film transistors," Applied physics letters, 100(10), p. 102108.

[186] Park, H.-G., Byun, S.-U., Jeong, H.-C., Lee, J.-W., and Seo, D.-S., 2013, "Photoreactive spacer prepared using electrohydrodynamic printing for application in a liquid crystal device," ECS Solid State Letters, 2(12), pp. R52-R54.

[187] Ahn, B. Y., Duoss, E. B., Motala, M. J., Guo, X., Park, S.-I., Xiong, Y., Yoon, J., Nuzzo, R. G., Rogers, J. A., and Lewis, J. A., 2009, "Omnidirectional printing of flexible, stretchable, and spanning silver microelectrodes," Science, 323(5921), pp. 1590-1593.

[188] Han, Y., and Dong, J., 2018, "Electrohydrodynamic (EHD) Printing of Molten Metal Ink for Flexible and Stretchable Conductor with Self‐Healing Capability," Advanced Materials Technologies, 3(3), p. 1700268.

[189] Jang, Y., Kim, J., and Byun, D., 2013, "Invisible metal-grid transparent electrode prepared by electrohydrodynamic (EHD) jet printing," Journal of Physics D: Applied Physics, 46(15), p. 155103.

[190] Teguh Yudistira, H., Pradhipta Tenggara, A., Dat Nguyen, V., Teun Kim, T., Dian Prasetyo, F., Choi, C.-g., Choi, M., and Byun, D., 2013, "Fabrication of terahertz metamaterial with high refractive index using high-resolution electrohydrodynamic jet printing," Applied Physics Letters, 103(21), p. 211106.

[191] Kress, S. J., Richner, P., Jayanti, S. V., Galliker, P., Kim, D. K., Poulikakos, D., and Norris, D. J., 2014, "Near-field light design with colloidal quantum dots for photonics and plasmonics," Nano letters, 14(10), pp. 5827-5833.

[192] Sutanto, E., Tan, Y., Onses, M. S., Cunningham, B. T., and Alleyne, A., 2014, "Electrohydrodynamic jet printing of micro-optical devices," Manufacturing Letters, 2(1), pp. 4-7.

[193] Vespini, V., Coppola, S., Todino, M., Paturzo, M., Bianco, V., Grilli, S., and Ferraro, P., 2016, "Forward electrohydrodynamic inkjet printing of optical microlenses on microfluidic devices," Lab on a Chip, 16(2), pp. 326-333.

[194] Onses, M. S., Ramírez-Hernández, A., Hur, S.-M., Sutanto, E., Williamson, L., Alleyne, A. G., Nealey, P. F., De Pablo, J. J., and Rogers, J. A., 2014, "Block copolymer assembly on nanoscale patterns of polymer brushes formed by electrohydrodynamic jet printing," Acs Nano, 8(7), pp. 6606-6613.

[195] Korkut, S., Saville, D. A., and Aksay, I. A., 2008, "Collodial cluster arrays by electrohydrodynamic printing," Langmuir, 24(21), pp. 12196-12201.

[196] Schneider, J., Rohner, P., Thureja, D., Schmid, M., Galliker, P., and Poulikakos, D., 2016, "Electrohydrodynamic nanodrip printing of high aspect ratio metal grid transparent electrodes," Advanced Functional Materials, 26(6), pp. 833-840.

[197] Lim, S., Park, S. H., An, T. K., Lee, H. S., and Kim, S. H., 2016, "Electrohydrodynamic printing of poly (3, 4-ethylenedioxythiophene): poly (4-styrenesulfonate) electrodes with ratio-optimized surfactant," RSC Advances, 6(3), pp. 2004-2010.

[198] Zheng, G., Sun, L., Wang, X., Wei, J., Xu, L., Liu, Y., Zheng, J., and Liu, J., 2016, "Electrohydrodynamic direct-writing microfiber patterns under stretching," Applied Physics A, 122(2), p. 112.

[199] Hanson Shepherd, J. N., Parker, S. T., Shepherd, R. F., Gillette, M. U., Lewis, J. A., and Nuzzo, R. G., 2011, "3D microperiodic hydrogel scaffolds for robust neuronal cultures," Advanced functional materials, 21(1), pp. 47-54.

List of figure captions:

Figure 1: High-resolution electrohydrodynamic (EHD) printing. (a) Schematic illustration of an EHD printing system. A voltage is connected to the nozzle and the electrode under the substrate to eject the ink with electrostatic force. (b) A typical nozzle and substrate configuration for EHD printing. Ink ejects from the apex of the conical meniscus that forms at the tip of the nozzle owing to the action of a voltage applied between the tip and ink, and the underlying substrate. These droplets eject onto a moving substrate to produce designed patterns. Reproduced with permission[17]. Copyright 2007, Nature Publishing Group. (c) Mechanism of EHD printing with typical forces acting on the fluid surface. Hydrodynamic force (F_h), which supplies fluid to the meniscus; the surface tension force (F_γ), which hangs the droplets on the capillary tip; and the electrostatic force (F_E), which deforms the meniscus into the cone shape and eject droplets or jet from the cone tip. S, L, G indicate the solid phase, liquid phase, and the gas phase, respectively. Reproduced with permission [31]. Copyright 2013, American Chemical Society.

Figure 2: Typical jetting modes of EHD printing. Reproduced with permission [22]. Copyright 1999, Springer Publishing.

Figure 3: (a) Phase diagram depicting flow transitions that occur as flow rate and/or electric field strength are varied. (b) Jetting maps showing the dependence of jetting modes on dimensionless parameters. Reproduced with permission [31]. Copyright 2013, American Chemical Society.

Figure 4: Effects of surface tension on proper jetting mode formation, for water, EG, DMSO, DMF, acetone, ethanol, and IPA. Reproduced with permission [54]. Copyright 2017, Wiley Publishing.

Figure 5: (a)Drop-on-demand EHD printed AgNP droplet. Reproduced with permission [58]. Copyright 2014, IOP Publishing. (b) Truncated hexagonal Au grid with a small lattice constant of 4μm. Reproduced with permission [196]. Copyright 2016, Wiley Publishing. (c) Optical micrographs of electroluminescence of green QD LEDs. Reproduced with permission [68]. Copyright 2015 American Chemical Society. (d) Printed PEDOT:PSS lines. Reproduced with permission [197]. Copyright 2016, The Royal Society of Chemistry. (e) Fluorescence

micrograph (left) and AFM image (right) of printed DNA microarrays. Reproduced with permission [81]. Copyright 2008, American Chemical Society. (f) Protein microarray formed by EHD printing. Reproduced with permission [82]. Copyright 2012, American Chemical Society. (g) DoD printed wax droplet. Reproduced with permission [115]. Copyright 2014, The American Society of Mechanical Engineers. (h) EHD printed PCL scaffold. Reproduced with permission [84]. Copyright 2013, IOP Publishing. (i) EHD directly printed 2D and 3D structures using molten metal alloys. Scale bar: 500 μm. Reproduced with permission[85, 188]. Copyright 2017, Elsevier Publishing. (j) EHD printed AgNW patterns. Reproduced with permission [95]. Copyright 2018, The Royal Society of Chemistry. (k) EHD printed RGO FETs. Reproduced with permission [96]. Copyright 2015, Wiley Publishing.

Figure 6: (a) Design concept of the double-layer FSP e-jet setup with corresponding electric field shaping, and printed patterns. Reproduced with permission [102]. Copyright 2014, American Institute of Physics. (b) Schematic of ring extractor design, and (c-e) the printed 3D micro-structures. Reproduced with permission [103]. Copyright 2017, IOP Publishing. (f) Principle scheme of the multi-nozzle multi-level voltage method (MVM), and (g) Printed droplets show good dimension consistency and position consistency. Reproduced with permission [107].Copyright 2015, American Institute of Physics.

Figure 7: (a) Image of a flower pattern formed with EHD printed dots (~8 μm diameters) of SWNTs from an aqueous solution. Reproduced with permission [17]. Copyright 2007, Nature Publishing Group. (b) High speed camera image of EHD DoD printing of silver nanocolloid using pulsed voltage. Reproduced with permission [117]. Copyright 2014, Springer Publishing. (c) Time-lapse image of EHP DoD of methanol solution with a constant DC voltage. Reproduced with permission [45]. Copyright 2004. The American Chemical Society.

Figure 8: (a) Schematic voltage profile for the pulsed EHD printing and the resulting jetting behavior. Reproduced with permission [99]. Copyright 2008, American Institute of Physics. (b) Schematic plot of AC-pulse modulated EHD-jet printing process. Residue charge of printed droplets is neutralized on insulating substrates, and (c) drop-on-demand printed droplets with

ejection frequency and droplet size controlled by parameter of the AC-pulse voltage. Reproduced with permission [58]. Copyright 2014, IOP Publishing.

Figure 9: (a) Stable cone-jet on the EHD printing of melted PLC. (b) EHD printed circular coil pattern. Reproduced with permission [84]. Copyright 2013, IOP Publishing. (c) The deposition behavior of PEO solution jet with different standoff distance. (d-f) Plotted PEO microfibers at different standoff distance. Reproduced with permission [198]. Copyright 2016, Springer Publishing.

Figure 10: (a) Scaling law shows the relationship between pulsation frequency and the scaled electric field. The slop of the data in this log-log plot is approximately ~1.5. (b) Images captured using a high-speed camera for these experiments to validate the scaling law. The time separation between adjacent images is 100 μs. Reproduced with permission [46]. Copyright 2008, American Institute of Physics.

Figure 11: (a) Schematic configuration for FEA modeling of the electrostatic force on the droplet and the electrical field distribution around the nozzle tip during the droplet ejection. Reproduced with permission [115]. Copyright 2014, The American Society of Mechanical Engineers. (b) The change of the tip-streaming from an uncharged, slightly conducting liquid drop subject to a uniform external electric field. Reproduced with permission [141]. Copyright 2013, National Academy of Science

Figure 12: (a) Electrohydrodynamic 3D printing using a phase change material (wax) as the ink. Reproduced with permission [104]. Copyright 2014, Elsevier Publishing. (b) Direct printing of silver pillars by auto-focusing EHD printing. Reproduced with permission [112]. Copyright 2012, Nature Publishing Group. (c) Schematic and SEM images of 3D wall structures made of anthracene and TIPS-pentacene. Reproduced with permission [152]. Copyright 2015, Wiley Publishing.

Figure 13: (a) EHD printed densely packed D15 on a narrow rectangle of patterned fibronectin and the printed spot which is small enough to constrain single cells. Scale bar: 50μm.

Reproduced with permission [164]. Copyright 2011, Wiley Publishing. (b) EHD printed spiral rectangular shape of the bacterial colony pattern. (c) bacterial pattern of the eagle. Scale bar: 2mm. Reproduced with permission. [159]. Copyright 2009, Springer Publishing. (d) Confocal images of primary rat hippocampal cells distributed within scaffold, primary monoclonal antibody for actin is used to label the processes (green), while TO-PRO3 was used to label nuclei (red). Reproduced with permission [199]. Copyright 2011, Wiley Publishing.

Figure 14: (a) Transparent thin film transistors with EHD printed semiconductors. Scale bar:300μm. Reproduced with permission [185]. Copyright 2012, American Institute of Physics. (b) Printed AgNW heaters and time response of the AgNW heater (scale bar, 5 mm). Reproduced with permission [95]. Copyright 2018, the Royal Society of Chemistry. (c) EHD printed conductor on PDMS, A stable electrical response was achieved during bending test. (d) EHD printed 20 x 20 matrix of touch sensors over a 10x10 mm area, the touch signal from each individual sensor was detected by the change in the capacitance. Reproduced with permission [188]. Copyright 2018, Wiley Publishing. (e) EHD printed reduced graphene oxide (RGO) with different thickness. Scale bar: 200μm. (f) High-resolution printing of (RGO) on nonplanar surfaces. Scale bar: 50 μm. (g) SEM images of the RGO patterns printed on the sidewall of a glass microcapillary as the substrate. Scale bars: 100 μm. Reproduced with permission [96]. Copyright 2015, Wiley Publishing.

Figure 15: (a) Cross-sectional view of polymer microlens on a surface after treatment using Fluorolink S10 providing a hydrophobic condition. (b) Representative image of a thin fluorinated layer onto a microfluidic chip with printed and cured lenses formed with different diameters of 150–1500 μm. (c) Optical microscope images of the polymer microlens on the microfluidic chip. (d) The polymeric microlens was positioned over the USAF target and observed under an optical microscope. (e1-e4) Microlenses were directly deposited on-board chip. Reproduced with permission [193]. Copyright 2016, The Royal Society of Chemistry.

Figure 16: Electrohydrodynamic jet printing of BCP films. (a) SEM images of a complex pattern printed with two PS-b-PMMAs with different MWs. The left and right images present high-magnification views. (b) Individual dots (left) and lines (right) printed with 37-37 K (top) and

25-26 K (bottom) PS-b-PMMA (0.1% ink and a nozzle with 500 nm internal diameter). (c) SEM image showing self-assembled nanoscale structures with two different morphologies (lamellae forming 37-37 K, left; cylinder forming 46-21 K, right) printed as lines. Reproduced with permission [80]. Copyright 2013, Nature Publishing Group.

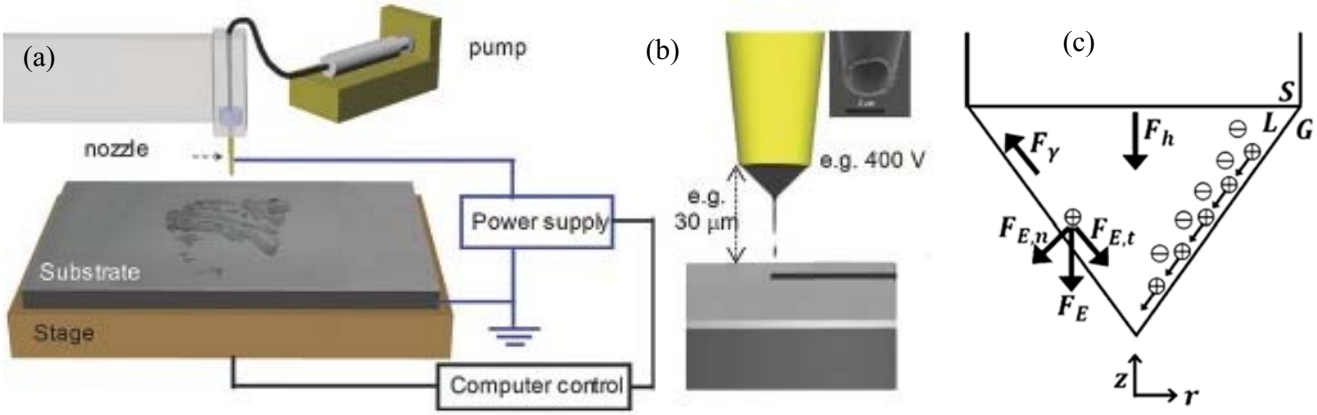

Figure 1: High-resolution electrohydrodynamic (EHD) printing. (a) Schematic illustration of an EHD printing system. A voltage is connected to the nozzle and the electrode under the substrate to eject the ink with electrostatic force. (b) A typical nozzle and substrate configuration for EHD printing. Ink ejects from the apex of the conical meniscus that forms at the tip of the nozzle owing to the action of a voltage applied between the tip and ink, and the underlying substrate. These droplets eject onto a moving substrate to produce designed patterns. Reproduced with permission [17]. Copyright 2007, Nature Publishing Group. (c) Mechanism of EHD printing with typical forces acting on the fluid surface. Hydrodynamic force (F_h), which supplies fluid to the meniscus; the surface tension force (F_γ), which hangs the droplets on the capillary tip; and the electrostatic force (F_E), which deforms the meniscus into the cone shape and eject droplets or jet from the cone tip. S, L, G indicate the solid phase, liquid phase, and the gas phase, respectively. Reproduced with permission [31]. Copyright 2013, American Chemical Society.

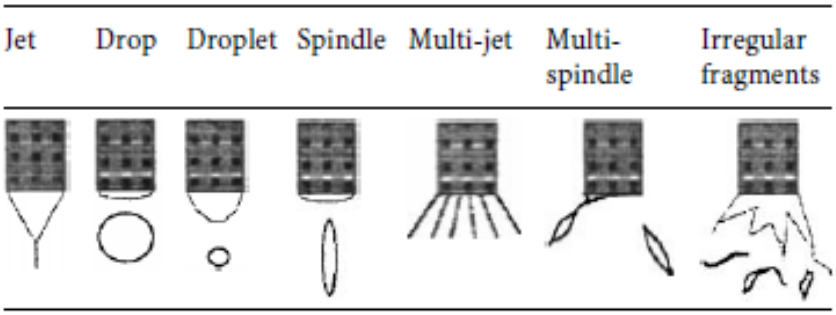

Figure 2: Typical jetting modes of EHD printing. Reproduced with permission [22]. Copyright 1999, Springer Publishing.

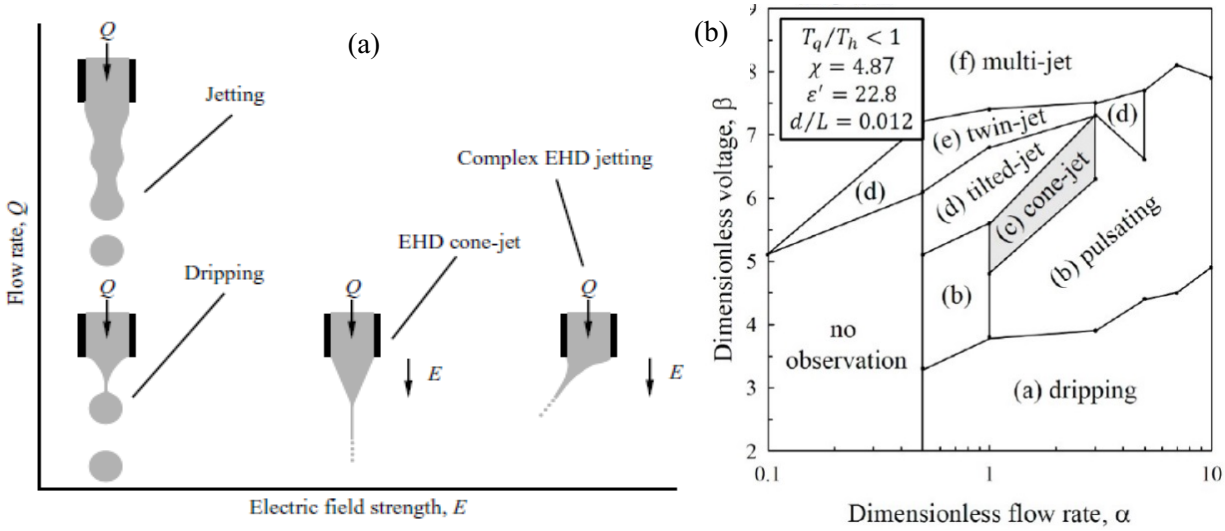

Figure 3: (a) Phase diagram depicting flow transitions that occur as flow rate and/or electric field strength are varied. (b) Jetting maps showing the dependence of jetting modes on dimensionless parameters. Reproduced with permission [31]. Copyright 2013, American Chemical Society.

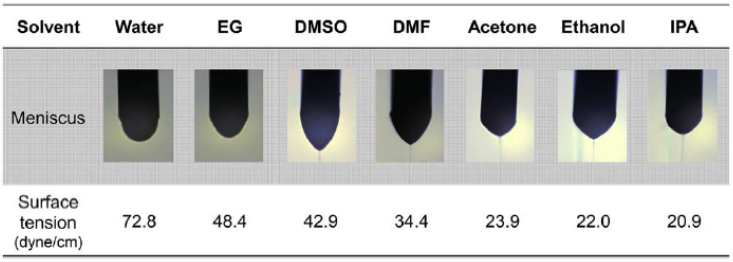

Figure 4: Effects of surface tension on proper jetting mode formation, for water, EG, DMSO, DMF, acetone, ethanol, and IPA. Reproduced with permission [54]. Copyright 2017, Wiley Publishing.

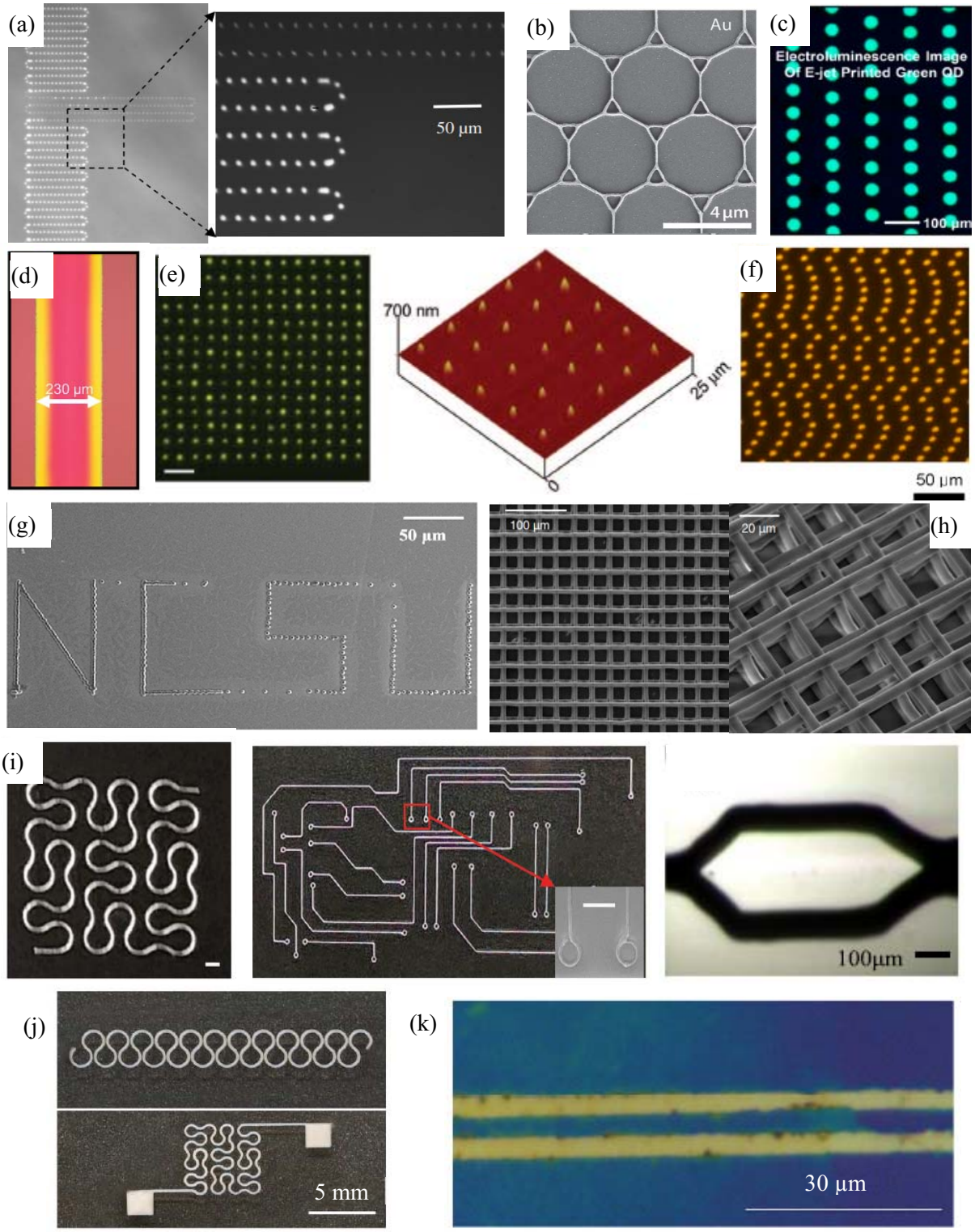

Figure 5: (a) Drop-on-demand EHD printed AgNP droplet. Reproduced with permission [58]. Copyright 2014, IOP Publishing. (b) Truncated hexagonal Au grid with a small lattice constant of 4μm. Reproduced with permission [196]. Copyright 2016, Wiley Publishing. (c) Optical micrographs of electroluminescence of green QD LEDs. Reproduced with permission [68]. Copyright 2015 American Chemical Society. (d) Printed PEDOT:PSS lines. Reproduced with permission [197]. Copyright 2016, The Royal Society of Chemistry. (e) Fluorescence micrograph (left) and AFM image (right) of printed DNA microarrays. Reproduced with permission [81]. Copyright 2008, American Chemical Society. (f) Protein microarray formed by EHD printing. Reproduced with permission [82]. Copyright 2012, American Chemical Society. (g) DoD printed wax droplet. Reproduced with permission [115]. Copyright 2014, The American Society of Mechanical Engineers. (h) EHD printed PCL scaffold. Reproduced with permission [84]. Copyright 2013, IOP Publishing. (i) EHD directly printed 2D and 3D structures using molten metal alloys. Scale bar: 500 μm. Reproduced with permission [85, 188]. Copyright 2017, Elsevier Publishing. (j) EHD printed AgNW patterns. Reproduced with permission [95]. Copyright 2018, The Royal Society of Chemistry. (k) EHD printed RGO FETs. Reproduced with permission [96]. Copyright 2015, Wiley Publishing.

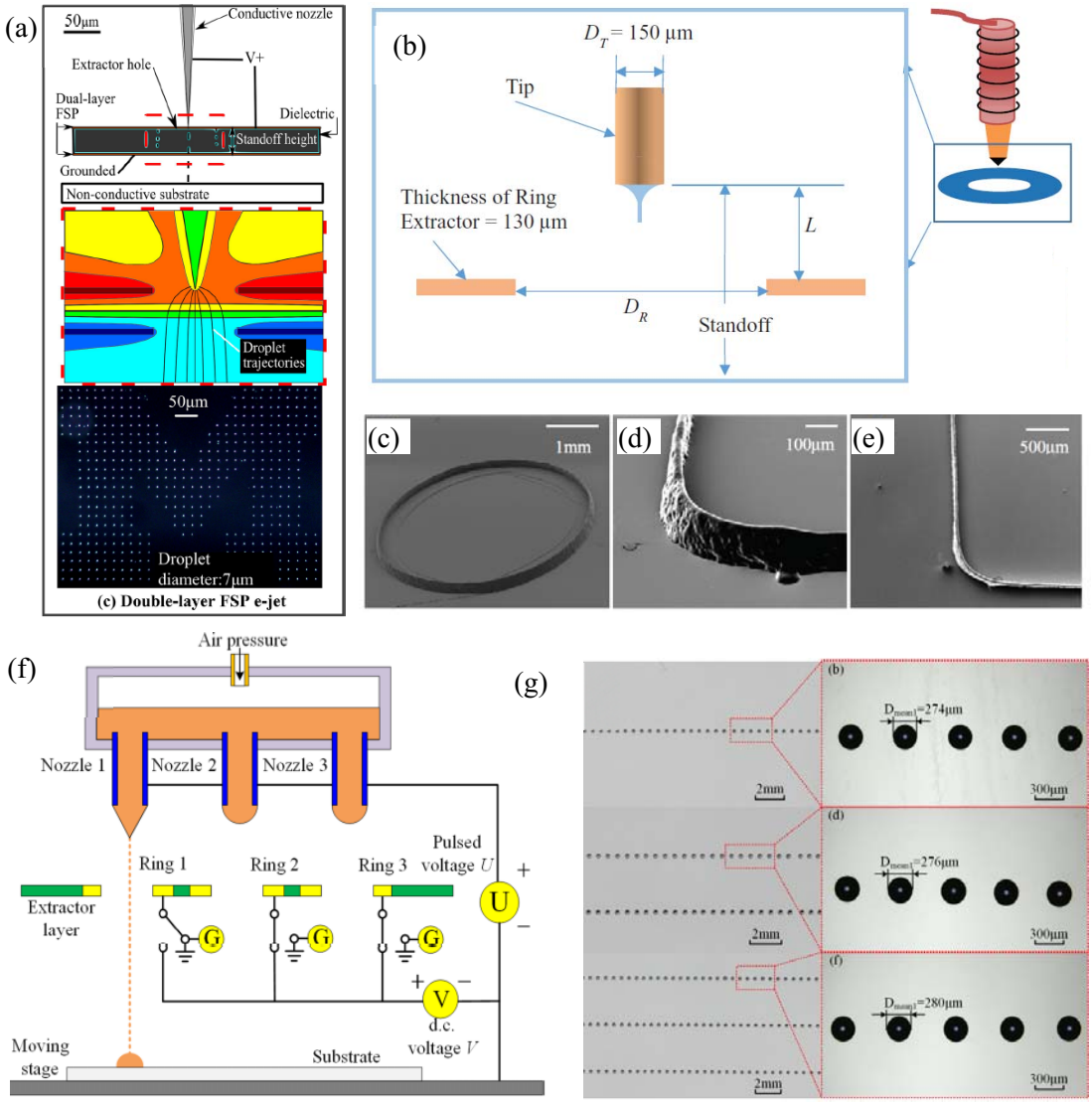

Figure 6: (a) Design concept of the double-layer FSP e-jet setup with corresponding electric field shaping, and printed patterns. Reproduced with permission [102]. Copyright 2014, American Institute of Physics. (b) Schematic of ring extractor design, and (c-e) the printed 3D micro-structures. Reproduced with permission [103]. Copyright 2017, IOP Publishing. (f) Principle scheme of the multi-nozzle multi-level voltage method (MVM), and (g) Printed droplets show good dimension consistency and position consistency. Reproduced with permission [107]. Copyright 2015, American Institute of Physics.

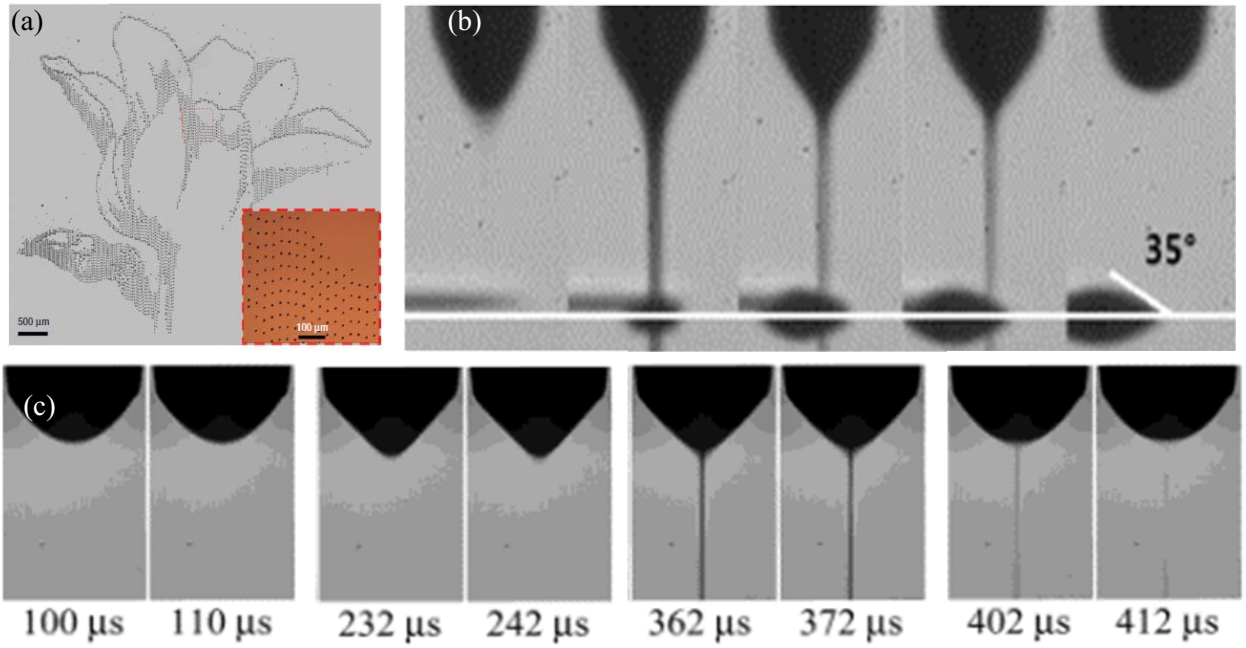

Figure 7: (a) Image of a flower pattern formed with EHD printed dots (~8 µm diameters) of SWNTs from an aqueous solution. Reproduced with permission [17]. Copyright 2007, Nature Publishing Group. (b) High speed camera image of EHD DoD printing of silver nanocolloid using pulsed voltage. Reproduced with permission [117]. Copyright 2014, Springer Publishing. (c) Time-lapse image of EHP DoD of methanol solution with a constant DC voltage. Reproduced with permission [45]. Copyright 2004. The American Chemical Society.

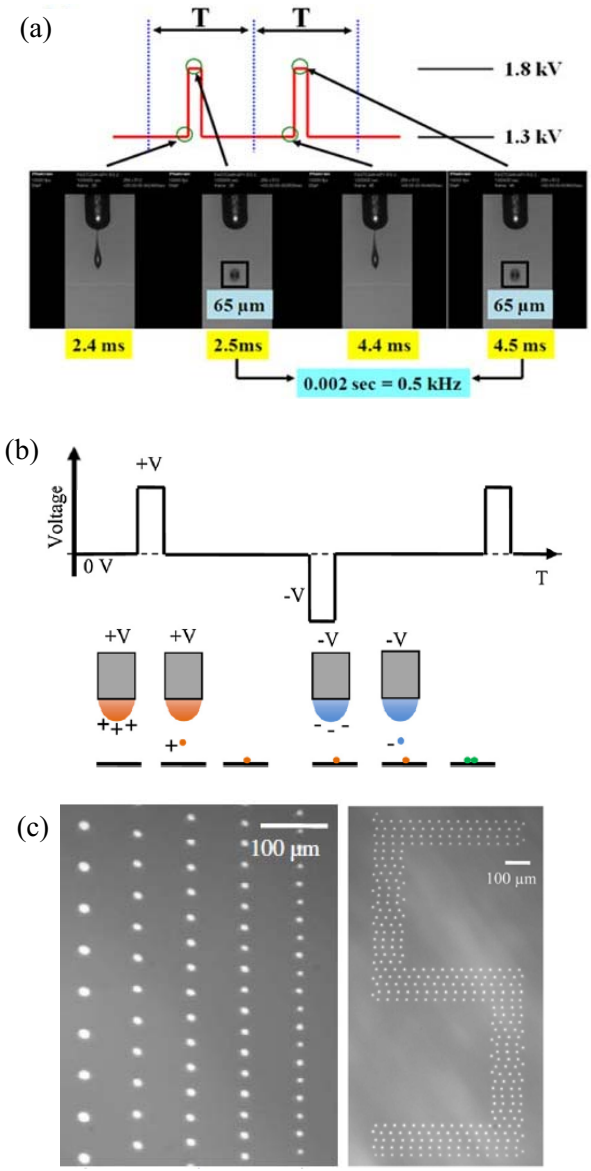

Figure 8: (a) Schematic voltage profile for the pulsed EHD printing and the resulting jetting behavior. Reproduced with permission [99]. Copyright 2008, American Institute of Physics. (b) Schematic plot of AC-pulse modulated EHD-jet printing process. Residue charge of printed droplets is neutralized on insulating substrates, and (c) drop-on-demand printed droplets with ejection frequency and droplet size controlled by parameter of the AC-pulse voltage. Reproduced with permission [58]. Copyright 2014, IOP Publishing.

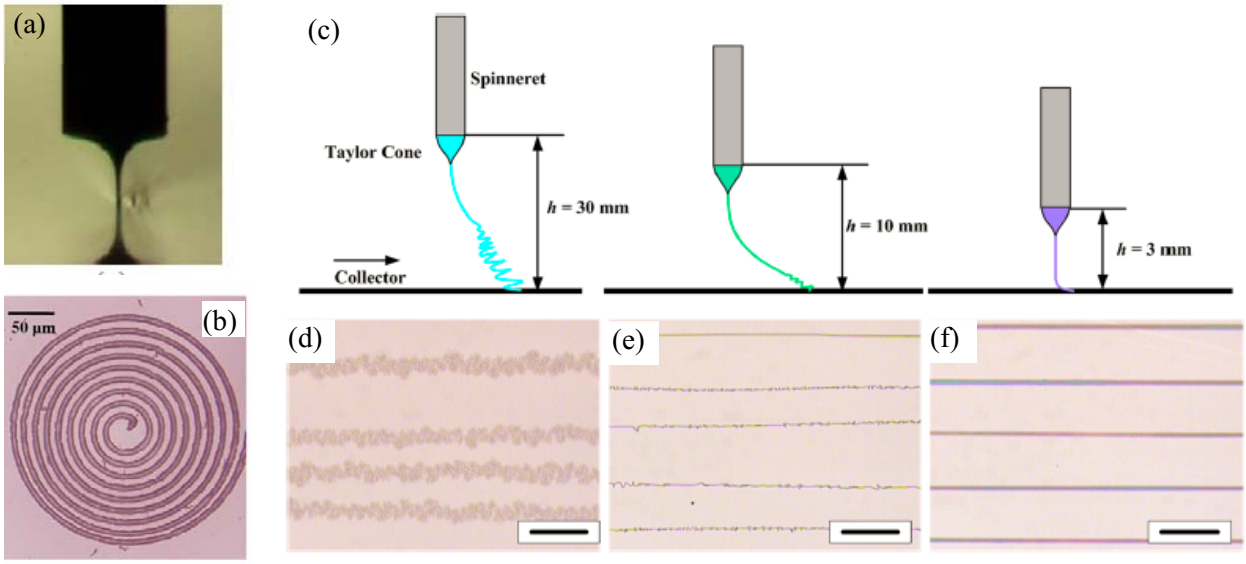

Figure 9: (a) Stable cone-jet on the EHD printing of melted PLC. (b) EHD printed circular coil pattern. Reproduced with permission [84]. Copyright 2013, IOP Publishing. (c) The deposition behavior of PEO solution jet with different standoff distance. (d-f) Plotted PEO microfibers at different standoff distance. Reproduced with permission [198]. Copyright 2016, Springer Publishing.

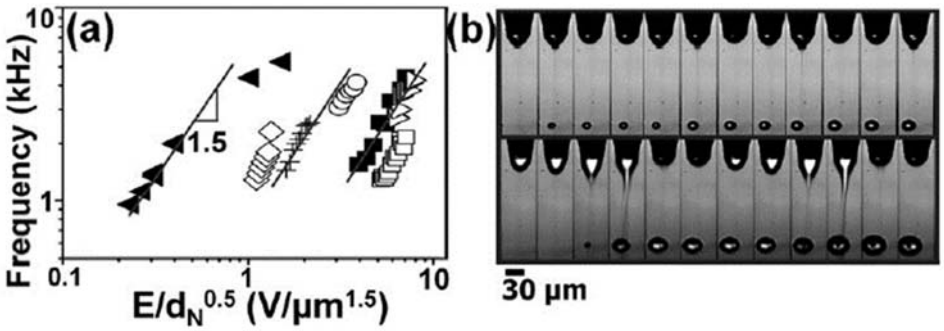

Figure 10: (a) Scaling law shows the relationship between pulsation frequency and the scaled electric field. The slop of the data in this log-log plot is approximately ~1.5. (b) Images captured using a high-speed camera for these experiments to validate the scaling law. The time separation between adjacent images is 100 μs. Reproduced with permission [46]. Copyright 2008, American Institute of Physics.

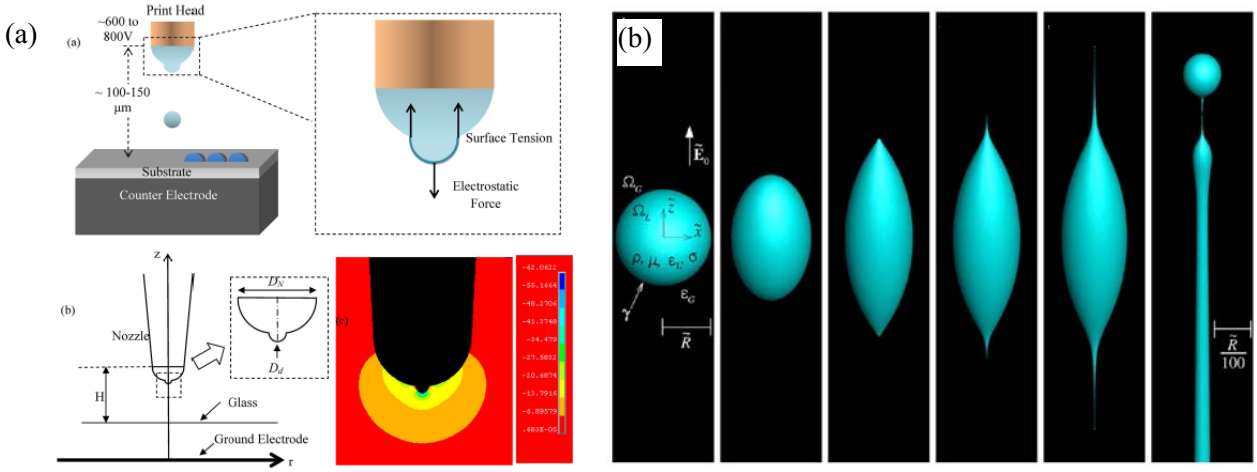

Figure 11: (a) Schematic configuration for FEA modeling of the electrostatic force on the droplet and the electrical field distribution around the nozzle tip during the droplet ejection. Reproduced with permission [115]. Copyright 2014, The American Society of Mechanical Engineers. (b) The change of the tip-streaming from an uncharged, slightly conducting liquid drop subject to a uniform external electric field. Reproduced with permission [141]. Copyright 2013, National Academy of Science

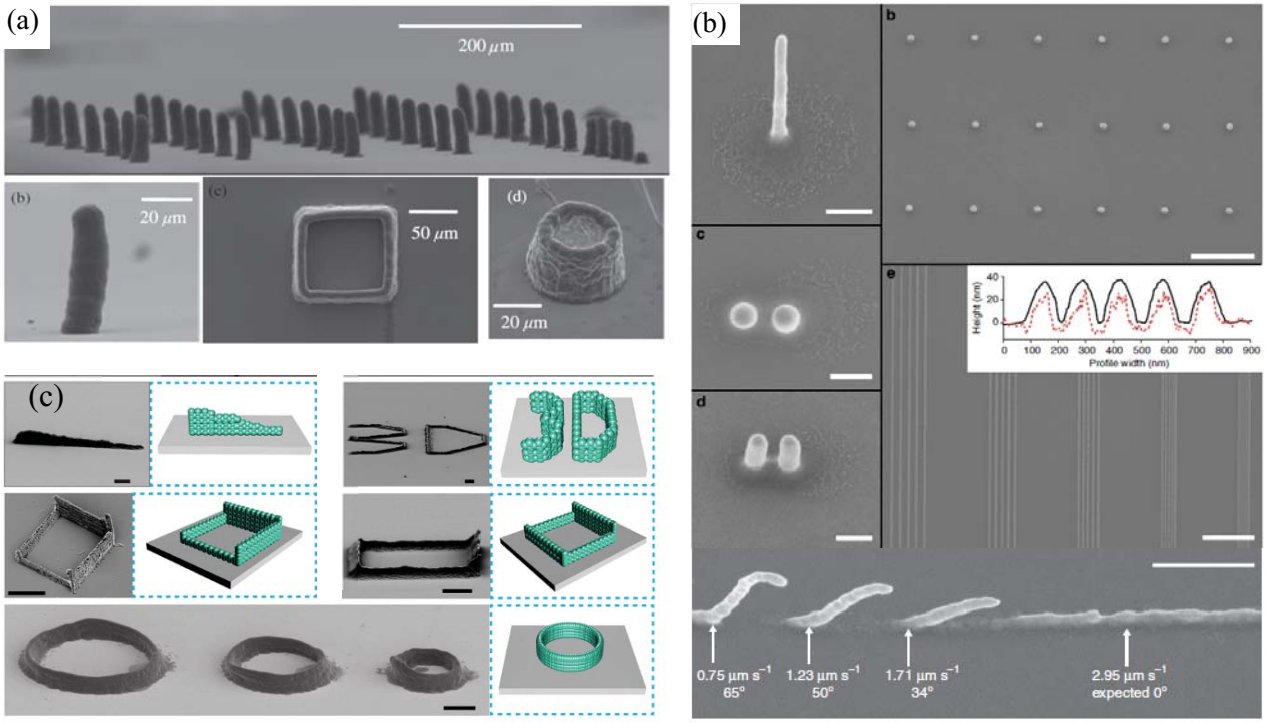

Figure 12: (a) Electrohydrodynamic 3D printing using a phase change material (wax) as the ink. Reproduced with permission [104]. Copyright 2014, Elsevier Publishing. (b) Direct printing of silver pillars by auto-focusing EHD printing. Reproduced with permission [112]. Copyright 2012, Nature Publishing Group. (c) Schematic and SEM images of 3D wall structures made of anthracene and TIPS-pentacene. Reproduced with permission [152]. Copyright 2015, Wiley Publishing.

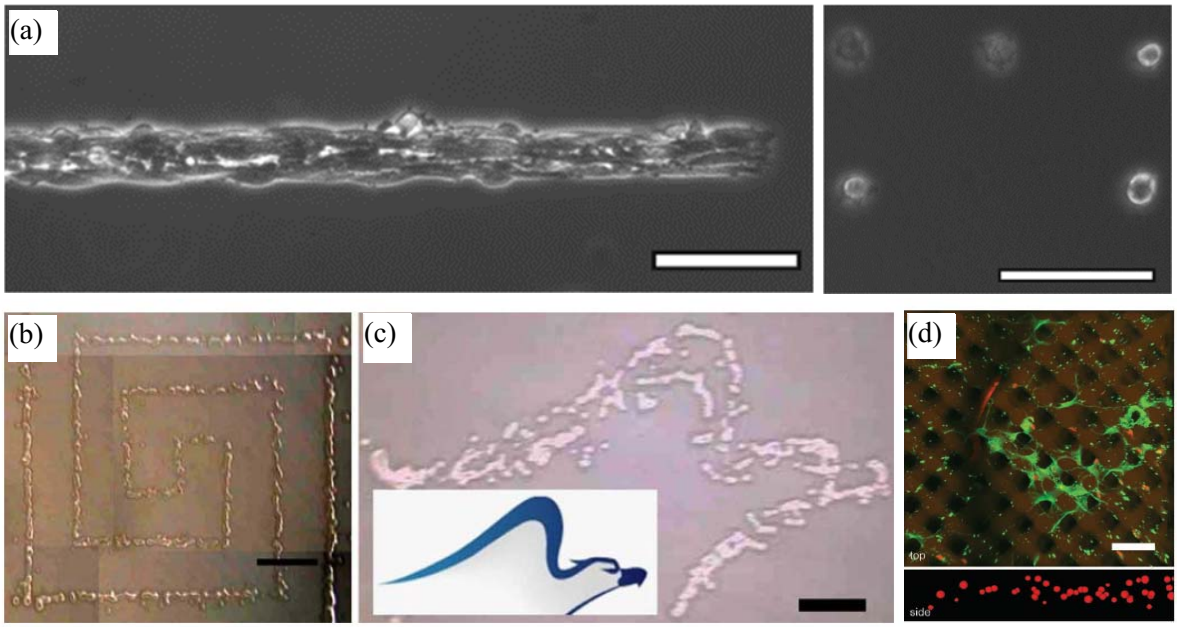

Figure 13: (a) EHD printed densely packed D15 on a narrow rectangle of patterned fibronectin and the printed spot which is small enough to constrain single cells. Scale bar: 50µm. Reproduced with permission [164]. Copyright 2011, Wiley Publishing. (b) EHD printed spiral rectangular shape of the bacterial colony pattern. (c) bacterial pattern of the eagle. Scale bar: 2mm. Reproduced with permission. [159]. Copyright 2009, Springer Publishing. (d) Confocal images of primary rat hippocampal cells distributed within scaffold, primary monoclonal antibody for actin is used to label the processes (green), while TO-PRO3 was used to label nuclei (red). Reproduced with permission [199]. Copyright 2011, Wiley Publishing.

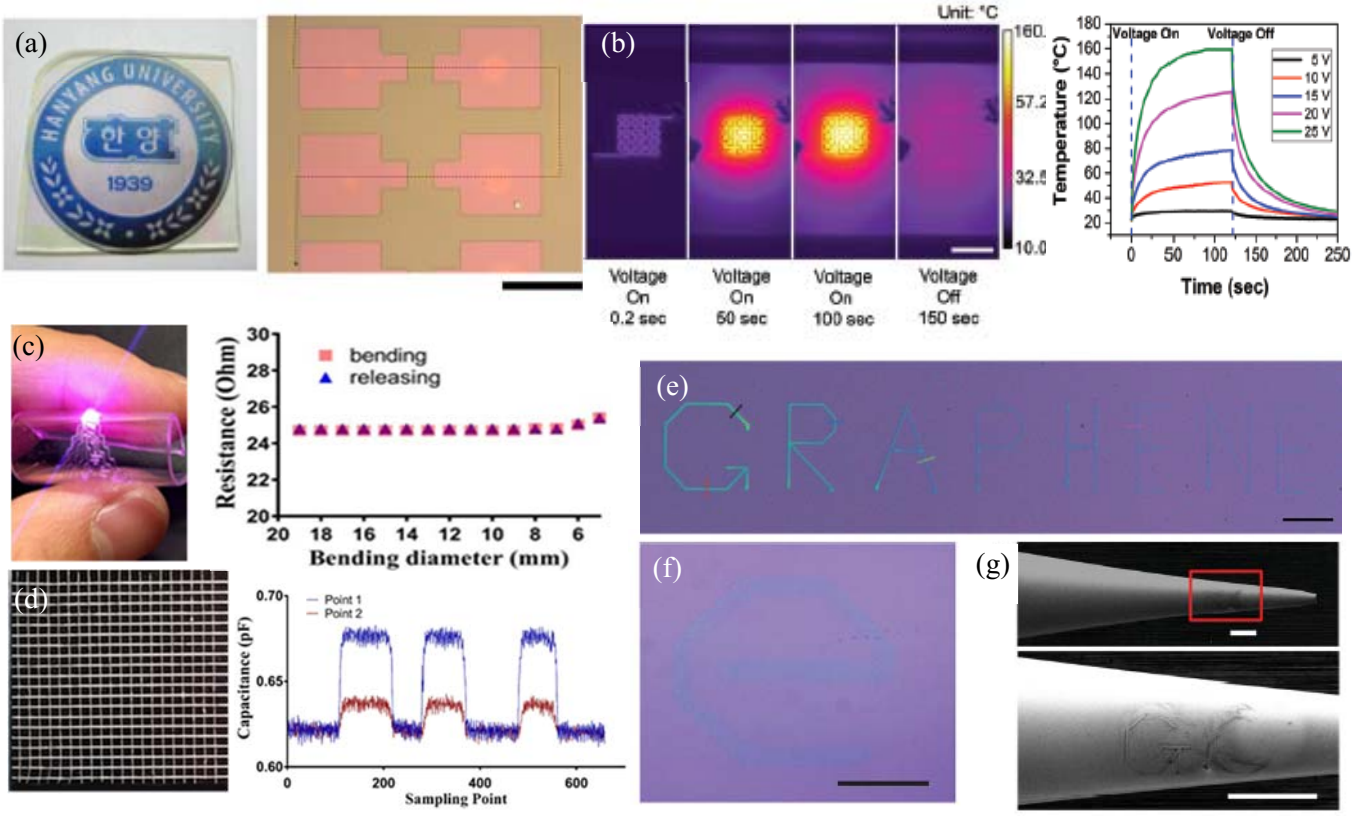

Figure 14: (a) Transparent thin film transistors with EHD printed semiconductors. Scale bar:300µm. Reproduced with permission [185]. Copyright 2012, American Institute of Physics. (b) Printed AgNW heaters and time response of the AgNW heater (scale bar, 5 mm). Reproduced with permission [95]. Copyright 2018, the Royal Society of Chemistry. (c) EHD printed conductor on PDMS, A stable electrical response was achieved during bending test. (d) EHD printed 20 x 20 matrix of touch sensors over a 10x10 mm area, the touch signal from each individual sensor was detected by the change in the capacitance. Reproduced with permission [188]. Copyright 2018, Wiley Publishing. (e) EHD printed reduced graphene oxide (RGO) with different thickness. Scale bar: 200µm. (f) High-resolution printing of (RGO) on nonplanar surfaces. Scale bar: 50 µm. (g) SEM images of the RGO patterns printed on the sidewall of a glass microcapillary as the substrate. Scale bars: 100 µm. (e-g) Reproduced with permission [96]. Copyright 2015, Wiley Publishing.

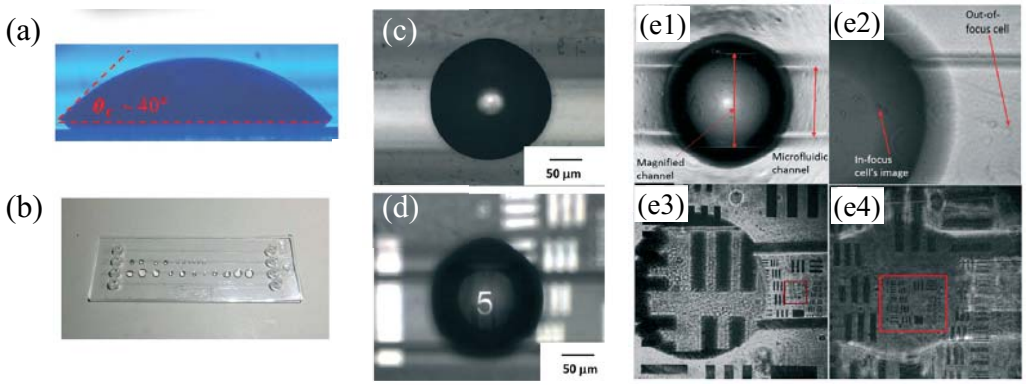

Figure 15: (a) Cross-sectional view of polymer microlens on a surface after treatment using Fluorolink S10 providing a hydrophobic condition. (b) Representative image of a thin fluorinated layer onto a microfluidic chip with printed and cured lenses formed with different diameters of 150–1500 µm. (c) Optical microscope images of the polymer microlens on the microfluidic chip. (d) The polymeric microlens was positioned over the USAF target and observed under an optical microscope. (e1-e4) Microlenses were directly deposited on-board chip. Reproduced with permission [193]. Copyright 2016, The Royal Society of Chemistry.

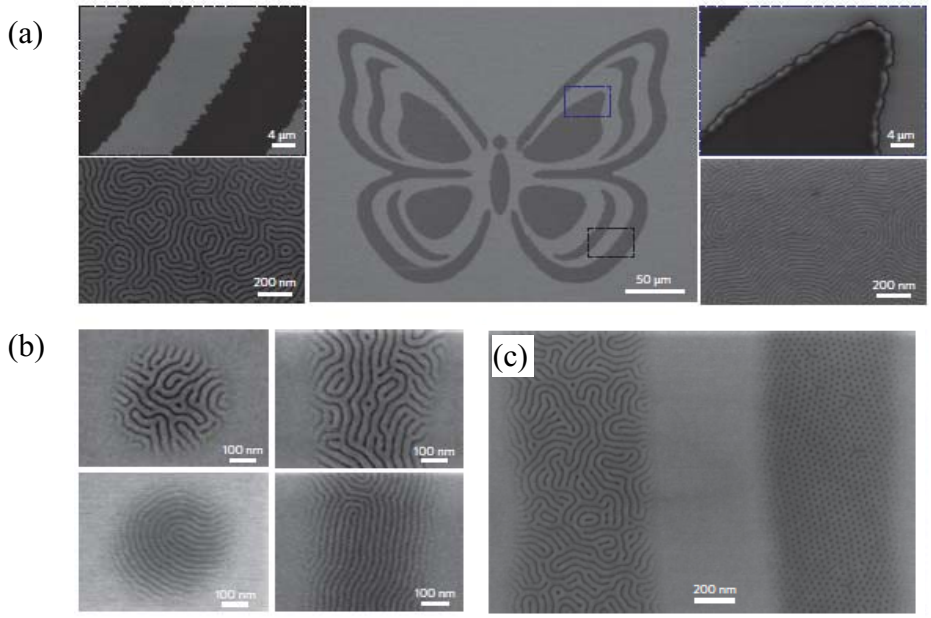

Figure 16: Electrohydrodynamic jet printing of BCP films. (a) SEM images of a complex pattern printed with two PS-b-PMMAs with different MWs. The left and right images present high-magnification views. (b) Individual dots (left) and lines (right) printed with 37-37 K (top) and 25-26 K (bottom) PS-b-PMMA (0.1% ink and a nozzle with 500 nm internal diameter). (c) SEM image showing self-assembled nanoscale structures with two different morphologies (lamellae forming 37-37 K, left; cylinder forming 46-21 K, right) printed as lines. Reproduced with permission [80]. Copyright 2013, Nature Publishing Group.